Fermi National Accelerator Laboratory

FERMILAB-Conf-82/87
2000.000

TRANSVERSE MOMENTUM SPECTRA OF DIMUONS PRODUCED IN HADRONIC INTERACTIONS AND COMPARISON WITH QCD*

P. K. Malhotra

December 1982

*Invited review talk given at the Workshop on Drell-Yan Processes, Fermilab, October 7-8, 1982

TRANSVERSE MOMENTUM SPECTRA OF DIMUONS PRODUCED IN HADRONIC INTERACTIONS AND COMPARISON WITH QCD

P.K. Malhotra*
Fermi National Accelerator Laboratory
P.O. Box 500, Batavia, IL 60510

Abstract

We have reviewed comprehensively the data on the transverse momentum spectra (p_T) of high mass lepton pairs produced in hadronic interactions. The data are extensively compared with the predictions of Quantum Chromo Dynamics to $O(\alpha_s)$, including some $O(\alpha_s^2)$ effects through the use of a p_T independent K factor. Sensitivity of the calculations to variations in the parameters used is discussed. A compilation of the K factor is given. Possible nuclear effects which can contribute to cross section or alter differential distributions in p_T, x_F or mass for the dimuon production in nuclear targets are discussed. Linear fits to the data on $\langle p_T^2 \rangle$ vs. s and $\langle p_T \rangle$ vs. $\sqrt{s}$ for π^-N and pN reactions are presented. Using the average value of the intrinsic transverse momentum squared deduced from fits to $\langle p_T^2 \rangle$ vs. s, predictions of the QCD are calculated and compared with the data. An important conclusion arrived at is that QCD to $O(\alpha_s)$ is not able to account for the observed features of the p_T distributions in a satisfactory manner.

*On leave from the Tata Institute of Fundamental Research, Homi Bhabha Road, Bombay-400-005, India

Invited review talk given at the Workshop on Drell-Yan Processes, Fermilab, October 7-8, 1982.

1. Introduction

Interest in dimuon ($\mu^+\mu^-$ pairs) production in hadron-hadron interactions began with the pioneering experiment of Lederman and his collaborators[1] in 1970. This field received a big boost from Drell and Yan[2] who suggested a quark-antiquark annihilation mechanism based on parton model for the dimuon continuum. The early experiments provided a strong support for this simple picture. Some of the predictions of the model which have been verified are approximate scaling, charge asymmetry, linear dependence of the cross section on mass number A of the target and angular distribution. However, it is now well established that this model is unable to account for the absolute normalization and the high average transverse momentum (p_T) of the dimuons. This last feature has led to the Drell-Yan model giving way to the Quantum Chromo Dynamics (QCD) because of the inherent mechanism of gluon emission and absorption which provides a natural source for high p_T of the dimuons. Because of this reason and uniqueness of the signal, the production of high mass lepton pairs is regarded as one of the most important testing ground for the ideas of QCD.

The main aim of this talk is to review the data on transverse momentum spectra of dimuons and to confront it with the predictions of the QCD to $O(\alpha_s)$ including some $O(\alpha_s^2)$ correction (α_s is the QCD running coupling constant). We shall see that the QCD to $O(\alpha_s)$ is unable to account for the p_T spectra convincingly and that it is necessary to include higher order effects including those due to soft gluon emission.

For a more complete understanding of the field of dimuon production, the reader is advised to refer also to some recent reviews[3-6] and rapporteur talks [7-11].

2. Experiments - recent, current and near future.

Table 1 gives a summary of the dimuon continuum experiments[12-23]. Some of these experiments [13-15,20,23,24] have provided valuable data on the transverse momentum spectra of dimuons. Experiments NA10[19] at CERN, E326[17] and E615[18] at Fermilab have accumulated a fair amount of data which is now being analysed. Experiment E605[22] has had a short run in 1982 and is expected to run in 1983 with beams from the Tevatron-II.

3. QCD formalism

In this section we shall present the QCD formalism with which the data will be compared.

3.1 Leading order QCD expression for dimuon production

The dimuon differential cross section integrated over p_T to leading order (i.e. order $\alpha_s(Q^2)\ \ln Q^2$) is given by[25]

$$\frac{d\sigma(s,M^2y)}{dMdy} = \frac{8\pi\alpha^2\tau}{9M^3} \sum_i e_i^2 \left[q_i^{h_1}(x_1,Q^2)\bar{q}_i^{h_2}(x_2,Q^2)+(1\leftrightarrow 2)\right] \quad (1)$$

and

$$\frac{d\sigma(s,M^2,y)}{dMdx_F} = \frac{8\pi\alpha^2\tau}{9M^3} \frac{1}{(x_F^2+4\tau)^{1/2}} \sum_i e_i^2 \left[q_i^{h_1}(x_1,Q^2)\bar{q}_i^{h_2}(x_2,Q^2) + (1 \leftrightarrow 2) \right] \quad (2)$$

where, $y=\ln((E+p_\ell)/M_T)$, $M_T=(P_T^2+M^2)^{1/2}$

$\tau=M^2/s = x_1x_2$, $Q^2=M^2$

$x_F=2p_\ell/\sqrt{s} = x_1 - x_2$

$x_{1,2}=(x_F^2+4\tau)^{1/2}/2 \pm x_F = \sqrt{\tau}\, e^{\pm y}$,

and where the $q_i(x,Q^2)$ are the QCD evolved parton distribution functions as obtained from the deep inelastic lepton-proton scattering experiments.

The expression (1) and (2) are the same as the Drell-Yan expressions corresponding to the diagram of Fig. 1(a) except that the distributions have now acquired a Q^2 dependence.

It is now well established[15] that although the eqs. (1) and (2) do manage to reproduce the shapes of the experimental distributions, the experimental cross sections are higher than the predictions by a factor K=1.6-2.6 (see the compilation in Sect. 3.3).

3.2 Transverse momentum dependence in perturbative QCD to order α_s

In the simplest version of Drell-Yan model (Fig. 1(a)) the dimuons have no transverse momentum. However, since the annihilating quarks are confined inside a hadron they are expected to have some intrinsic transverse momentum (k_T), whose vector sum

will be the transverse momentum of the lepton pair. There is evidence[26] that $\langle k_T^2 \rangle = 0.16$ (GeV/c)^2 and therefore $\langle p_T^2 \rangle$ of the lepton pairs from this contribution will be only 0.32 (GeV/c)^2. Moreover, if k_T is indepenent of the parton's x, then $\langle p_T \rangle$ will be indepenent of x_F and of M except near kinematic boundaries. However, the observed $\langle p_T^2 \rangle$ is much larger than $\langle k_T^2 \rangle$ and furthermore, $\langle p_T^2 \rangle$ clearly increases linearly with s. These features are qualitatively expected on the basis of QCD to $O(\alpha_s)$. The hope was that this would be adequate to explain the data even at the quantitative level. As we shall show later this is not the case.

The $O(\alpha_s)$ diagrams are shown in Figs. 1(b) and 1(c). The perturbative expression for differential cross section to $O(\alpha_s)$ for dimuon production can be written as[27] (we assume $Q^2=M^2$)

$$\frac{d\sigma_p(s,M^2,y,p_T)}{dM\ dy\ dp_T^2} = \frac{16\alpha^2}{27}\frac{s}{M}\int_{x_1 min}^{1} dx_1 \frac{x_1 x_2 \alpha_s}{x_1 s+u-M^2}\frac{(\hat{t}-M^2)^2+(\hat{u}-M^2)^2}{\hat{s}^2\hat{t}\hat{u}}$$

$$\cdot \sum_i e_i^2\left[q_i^{h_1}(x_1,Q^2)\ \bar{q}_i^{h_2}(x_2,Q^2)+(1\leftrightarrow 2)\right]$$

$$+\frac{2\alpha^2}{9}\frac{s}{M}\int_{x_1 min}^{1} dx_1\ \frac{x_1 x_2 \alpha_s}{x_1 s+u-M^2}\ \frac{\hat{s}^2+\hat{u}^2+2M^2\hat{t}}{-\hat{s}^3\ \hat{u}}$$

$$\cdot \sum_i e_i^2\left[q_i^{h_1}(x_1,Q^2)\ G_i^{h_2}(x_2,Q^2)+(1\leftrightarrow 2)\right] \qquad (3)$$

where q_i's and G_i's are quark and gluon distribution functions, and

$$x_1^{min} = -u/(s+t-M^2),\ x_2=(-x_1 t-(1-x_1)M^2)/(x_1 s+u-M^2)$$
$$t= M^2-\sqrt{s}\, M_T\, e^{-y},\ u=M^2-\sqrt{s}\, M_T e^{y},$$
$$s= x_1 x_2 s,\ t=x_1 t+(1-x_1)M^2,\ u=x_2 u+(1-x_2)M^2,$$
$$M_T^2= p_T^2+M^2 \text{ and } \alpha_s=12\pi/(25\ \ln(Q^2/\Lambda^2)) .$$

The expression (3) is useful only for large p_T since it has a singularity at $p_T=0$. Furthermore, it ignores the intrinsic transverse momentum (k_T) of the parton. Altarelli, Parisi and Petronzio[28] have given a prescription which uses the intrinsic k_T to regularize the $p_T=0$ divergence leading to

$$\frac{d\sigma}{dMdydp_T^2} = \int d^2q_T \frac{d\sigma_P}{dMdydp_T^2}\left[f(\vec{p}_T-\vec{q}_T)-f(p_T)\right]$$
$$+ \pi\, f(p_T)\ \frac{d\sigma_{DY}}{dMdy} \quad . \qquad (4)$$

Here $\vec{q}_T=\vec{p}_T-\vec{k}_T$, σ_{DY} is the Drell-Yan cross section (with Q^2 dependent distribution functions) as given by eq. (1) and f represents the soft k_T distribution which is assumed to have a gaussian form with the normalization:

$$\int f(k_T)d^2k_T = \int d^2k_T\ \left(\exp -k_T^2/(4B^2)\right)\ /(4\pi B^2) = 1 \qquad (5)$$

Note that integration of the expression (4) over p_T yields just the Drell-Yan cross section (eq. 1).

3.3 K-factor

Although the Drell-Yan formula is able to reproduce the shape of the experimental distribution for $d\sigma/dMdy$, the experimental cross section is higher than the prediction by the so-called K-factor, i.e.

$$K = \text{(Observed cross section)}/\text{(Drell-Yan prediction)}.$$

The suggestion for the existence of the K-factor was made most clearly by the NA3 Collaboration[15], although the results of the CFS Collaboration[20] could also be interpreted in the same manner. In Table 2 we have compiled the existing measurement of the K-factor. The values range between 1.6 and 2.6. Although the errors are large there is some indication that the value of the K-factor for pN reactions may be somewhat smaller than that for $\pi^{\pm}$N reactions.

In principle, several effects could get folded into the determination of the K factor. For example, nuclear effects could contribute to the K factor (see sect. 9). The fact that the values of K with hydrogen and nuclear targets are of about the same magnitude would lead us to conclude that overall this is not a large effect (<25%). The experiments with pion beams could in principle suffer from the lack of an independent knowledge of the pion structure functions. But the fact that π^{+}N and π^{-}N reactions yield about the same value of K leads to the conclusion that the contribution due to this uncertainty can not be significant

($<$10%). Since the K factor deduced from the difference of $\sigma(\pi^- N)$ and $\sigma(\pi^+ N)$ has a similar value, it rules out any significant hadronic contribution to the dimuon continuum since it would largely cancel out in the difference. Thus, we conclude that the existence of the K factor can be considered to be fairly well established.

Theoretical explanation for the K factor has been provided by several authors[29] who have carried out the so-called full order α_s calculation. These calculations yield a value of K of the order of 1.8-2.0 independent of $\tau=M^2/s$ for $\tau \lesssim 0.5$. The origin of this large correction lies in the fact that whereas one uses structure functions defined for the deep inelastic scattering process, there are suttle differences between this and the Drell-Yan process. The full $O(\alpha_s)$ calculation leads to two large terms. The first is the famous π^2 term which arises from the continuation of the form factor from space-like to time-like values of Q^2. This term is associated with the vertex correction diagram. Its contribution decreases with τ and dominates for $\tau \lesssim 0.3$. The second term is associated with the phase space effects in the soft gluon emission from the initial $q\bar{q}$ pair. There is also a third term due to gluon Compton scattering, which is small and negative. The sum of all these terms leads to a value of K~1.8-2.0 which is almost constant for $\tau \lesssim 0.3$ i.e. in the range of the current experiments. Because of the nature of the origin of the different terms it is clear that the large correction is applicable mainly to the soft p_T distribution arising from the intrinsic p_T of the quarks.

A summary of the theoretical calculations[29,39] for the K factor is given in fig. 2. An important feature of these calculations is that the value of K is expected to increase dramatically for $\tau \gtrsim 0.5$, a region not easily accessible for experiments because of the rapidly falling cross section.

The $O(\alpha_s)$ correction is so large that it is necessary to carry out higher order calculations to ensure that the agreement is not destroyed. These calculations are difficult and only limited attempts have been made.

Ellis et.al.[30] have shown that for the non-singlet case, $\sigma(\pi^- N - \pi^+ N)$, the order α_s^2 diagrams lead to a fairly large correction to the p_T distribution given by

$$K'(p_T) = (d\sigma/dMdp_T^2)_{O(\alpha_s^2)+O(\alpha_s)} / (d\sigma/dMdp_T^2)_{O(\alpha_s)} \simeq 2. \qquad (6)$$

More correctly, K' decreases from about 2.3 at p_T=2.5 GeV/c to 1.8 at p_T=4.5 GeV/c. To our knowledge, no calculation has as yet been attempted for the singlet case which would be required, for example, for the reaction $pN \to \mu^+\mu^- X$. Nevertheless, we shall assume the validity of eq. (6) for pN as well as $\pi^- N$ reactions.

In view of the fact that $K'(p_T)$ and K have about the same values, we shall assume the K-factor to be independent of p_T. Furthermore, we shall use the K-factor as deduced from a comparison of the data with the Drell-Yan prediction. Although not strictly correct, in view of the above assumption our calculation can be considered to correspond to $O(\alpha_s^2)$ QCD.

4. Structure functions

The present knowledge of the structure functions has been reviewed recently by F. Eisele[31] and L. Lyons[3].

The nucleon structure functions for quarks have been determind by the CDHS collaboration from deep inelastic neutrino scattering experiments[32]. Since the Drell-Yan cross section (eq. 1) depends on the product of the quark structure function of one hadron and the antiquark structure function of the other hadron, the Drell-Yan mechanism can also be used to determine the structure functions [16,20,15]. In fact this is the best method known to determine the structure functions of $\pi^{\pm}$, $K^{\pm}$ etc. The NA3 collaboration[15] have used $\bar{p}N$-pN subtraction method to deduce the valence u and d quark structure functions for the proton since this difference is indepenent of the quark sea in the beam and the target. The results are consistent with those obtained by the CDHS collaboration from neutrino experiments, although the overall normalisation of the data is too high by a factor of ~2.3, the so-called K-factor. Similarly, the sea quark structure functions for the proton deduced from the dimuon experiments[20,15] are consistant with the CDHS results.

The valence, sea and gluon structure functions[15] for the proton used by us are as follow:

$$x\,u_p = u_o\, x^{0.52-0.16\,\bar{s}}(1-x)^{2.79+0.77\,\bar{s}}$$

$$x\,d_p = d_o\, x^{0.52-0.16\,\bar{s}}(1-x)^{3.79+0.77\,\bar{s}}$$

$$x\,S_p = (0.26+0.18\,\bar{s})(1-x)^{7.8+0.78\,\bar{s}}$$

$$x\,G_p = 3.06\,(1-x)^{5.0}$$

$$x\,V_\pi = V_o\,x^{0.4}(1-x)^{0.9}$$

$$x\,S_\pi = 0.24(1-x)^{6.9}$$

$$x\,G_\pi = 2.0(1-x)^{3.0}$$

where $\bar{s} = \ln\,[\ln(Q^2/0.25)/\ln(20/0.25)]$.

The valence and sea components for the proton are consistent with the CDHS results[32] and the gluon structure functions are based on counting rules. The proton structure functions given above imply that valence, quarks, sea quarks and antiquarks, and gluon carry 34%, 15% and 51% of the proton momentum at $Q^2=20\,(GeV/c)^2$. As Q^2 increases the valence and sea distributions become softer and the fractional momentum carried by valence quarks decreases to 30% and that carried by sea $q\bar{q}$ increases to 17% at $Q^2=70\ (GeV/c)^2$. The pion structure functions are those obtained by NA3[15]. We have assumed that $s\bar{s}$ pairs are suppressed by a factor of 2 compared to $u\bar{u}$ or $d\bar{d}$ pairs. The Q^2 dependence is small over the range of Q^2, $16<Q^2<70\ (GeV/c)^2$, of interest here. We shall later comment upon the effect of the Q^2-independent gluon structure function on the transverse momentum spectra of the dimuons.

5. QCD fits to the data on p_T spectra of the lepton pairs

We will now briefly outline the main ingredients of the QCD fits carried out by us. The differential cross section is given by eq. (4) together with eq. (1) and (3). This involves a time consuming k_T convolution over the annihilation and the Compton terms. Because of this it is not practical to do a minimisation

fit. The approach followed is to fix most of the parameters and to vary $\langle k_T^2 \rangle$ only. Although, we have identified $\langle k_T^2 \rangle$ with the contribution from the intrinsic transverse momentum of the partons, it includes possible other contributions as well.

The value of the scale parameter Λ in the QCD running coupling constant in not well known. Values ranging from 0.1 to 0.5 GeV/c have been obtained in the literature. Overall consensus[31] favors a value of $\Lambda \lesssim 0.35$ GeV/c. We have used in general a value Λ=0.5 GeV/c but have also indicated the effect on the results if a value of Λ=0.3 GeV/c or lower is used.

We use structure functions given in sect. 4 above. The K-factor is assumed to be independent of the transverse momentum of the dimuons and in this sense our calculation can be considered to be to order α_s^2 (see sect. 3).

The parameters Λ and $\langle k_T^2 \rangle$ are strongly correlated. Since, for a given Q^2, α_s increases, as Λ increases, a lower value of Λ would require a higher value of $\langle k_T^2 \rangle$ to fit the data.

5.1 $\underline{p\text{-}N \rightarrow \mu^+\mu^- x}$

Fig. 3,(a),(b) and (c) show the data of Columbia-Fermilab-Stony Brook Collaboration[20] for p_T spectra of the dimuons produced in p-Pt collisions at 400 GeV/c for M=5.5, 6.5, 7.5, 8.5 and 11.5 GeV and y=0.03. Also shown are QCD fits with Z/A=0.40, Λ=0.5 GeV/c, K=1.6 and $\langle k_T^2 \rangle$=0.88 $(\text{GeV/c})^2$. As can

be seen the fits are all quite good. The value of K=1.6 is also in good agreement with that obtained by Ito et al.[20] although they have used somewhat different structure functions. In this connection it should be mentioned that the authors quote a normalisation uncertainty of ±25%. The Q^2 dependence of the structure functions plays a significant role only for the M=11.5 GeV data.

Fig. 4 shows the data of CERN-MIT-LAPP-Harvard-Naples-Pisa Collaboration[23,24] for $pp \to \mu^+\mu^- X$ at $\sqrt{s}$=62 GeV and 44 GeV(ISR). These data sets are among the few available with a hydrogen target. The data at $\sqrt{s}$=44 GeV have not yet been published[24]. The authors have carried out fits of the form $d\sigma/dp_T^2 = A \cdot \exp(-\alpha p_T)$ for $p_T \gtrsim 0.5$ GeV/c.

Fig. 5 shows our QCD fits with K=1.8 and $\langle k_T^2 \rangle = 1.5$ $(GeV/c)^2$.

The main conclusions that we can draw from these fits are: (a) the fits require large values of $\langle k_T^2 \rangle$ and (b) the required value of $\langle k_T^2 \rangle$ increases with the beam energy.

5.2 Contributions of different terms and sensitivity to the parameters

The contributions of the different terms to the differential cross sections for 400 GeV/c pN collisions, M=7.5 GeV, y=0.03 are depicted in fig. 6. The solid line is the fit shown already in fig. 3(a). The curve labelled "intrinsic" corresponds to the

spectrum if only the non-perturbative contributions with $\langle k_T^2 \rangle = 0.88$ (GeV/c)^2 were present. The QCD contributions are clearly the dominant contributions beyond $p_T \sim 2$ GeV/c. The major contribution to the tail comes from the Compton term as expected for pN collisions.

The sensitivity to the Λ parameter can be seen by comparing the two curves for $\Lambda = 0.5$ and 0.3 GeV/c. The change in the differential cross section varies between 0 and about 18%. Fig. 7 shows the sensitivity to $\langle k_T^2 \rangle$ when its value is changed from 0.9 to 0.6 (GeV/c)^2, keeping Λ fixed at 0.5 GeV/c. The percentage change is about the same as for the above two values of Λ. Thus, Λ and $\langle k_T^2 \rangle$ are highly correlated. A lower value of Λ would require a higher value for $\langle k_T^2 \rangle$ to obtain an acceptable fit to the differential spectrum.

As mentioned in sect. 4 we have used gluon distribution based on quark counting rules. The gluon distribution given by Badier et al.[15] based on CDHS results is somewhat softer and has a fairly significant Q^2 dependence (becomes softer as Q^2 increases). If this were used the fit would require even higher values of $\langle k_T^2 \rangle$.

Since we have used a value of Λ (0.5 GeV/c) which is larger than indicated by experiments[31] and a gluon distribution which is harder than indicated by the CDHS results[32], the values of $\langle k_T^2 \rangle$ deduced in this study should be considered as lower bounds. The significance of this remark will have a bearing on our conclusions.

5.3 $\bar{p}N \rightarrow \mu^+\mu^- X$

The antiproton-nucleon annihilation is interesting because the dominant conribution to lepton production here comes from the valence partons in the initial state nucleons. Since the valence $\bar{q}$ distribution in an antiproton is identical to that for a valence q distribution in a proton, predictions are not affected by uncertainties in our knowledge of the nucleon sea.

There are only two experiments which have been done with $\bar{p}$ beams, E-537[14] at Fermilab and NA3[15] at CERN, but results on p_T distribution are so far available only from the former experiment. Fig. 8 shows the preliminary results from the experiment E537 on the transverse momentum distribution of dimuons ($4.0<M<8.5$ GeV, $y\geq 0$) in $\bar{p}W$ collisions at 125 GeV/c. The solid curve is the QCD fit with K=2.3 and $\langle k_T^2\rangle = 0.88$ $(GeV/c)^2$. The dominant contribution to the tail here comes from the annihilation term in contrast to the pN case where the Compton term provides the major contribution to the tail. A notewworthy feature is that because of the low projectile momentum the QCD contribution to the p_T is quite small.

5.4 $\pi^- N \rightarrow \mu^+\mu^- X$

In $\pi^- N$ collisions the dominant source of the dimuons is the annihilation of the valence $\bar{u}$ of the π^- and valence u's of the nucleon. An important difference between pN, $\bar{p}N$ and $\pi^- N$ collisions is that whereas in the first two one needs only the nucleon structure functions which are known from deep inelastic

scattering experiments, in the π^-N case one needs also the pion structure functions. But because the nucleon structure functions obtained using the Drell-Yan model agree with those obtained from the deep inelastic scattering experiments, one can use the Drell-Yan model to obtain the pion structure functions. Table 1 summarises the dimuon experiments with pion beams[12-19]. The data on p_T distributions is available mainly from NA3[15] and E-537[14] experiments.

Fig. 9 shows the preliminary results, from the experiment E537[14,33], on the p_T distributions of dimuons ($4.0<M$ 8.5 GeV, $y\geq 0$) in π^-N collisions at 125 GeV/c. The solid curve is the QCD fit with K=2.5 and $\langle k_T^2\rangle=0.88$ $(GeV/c)^2$. The quark structure functions for the π^- are those determined by NA3 collaboration and given in sect. 4. The sensitivity to the pion and nucleon sea is small as expected. The sea conribution is about 13% for M=4.5 GeV and only 2% for M=8.0 GeV. The tail of the p_T distribution clearly requires the QCD conribution which comes dominantly from the annihilation term as was found for the $\bar{p}N$ case.

Since the valence $\bar{u}$ distribution for π^- is much harder compared to valence antiquark distributions of the $\bar{p}$, the QCD annihilation term is relatively more important in the case of π^-N than in the case of $\bar{p}N$. The effect of the harder quark distributions in π^- compared to $\bar{p}$ is even more dramatic in the x_F distribution of the dimuon[14,33].

NA3 collaboration has provided some of the highest statistics data on the p_T distribution of dimuons in π^-N reactions. Figs. 10(a) and (b) show their new plots presented at the Paris Conference[15]. Fig. 11 shows their results for $\pi^- Pt \to \mu^+\mu^- X$ at 150 GeV/c for $y \geq -0.6$ and for $4.1<M<5$ GeV, $5<M<6$ GeV and $4.1<M<8.5$ GeV. Also shown are our QCD fits with K=2.3 and $\langle k_T^2 \rangle = 1.0$ (GeV/c)^2. Fig. 12 shows a comparison of the data[15] at 150,200 and 280 GeV/c, $y \geq -0.6$ and $4.1<M<8.5$ GeV together with our QCD fits (K=2.3). The fits require values of $\langle k_T^2 \rangle = 1.0$, 1.1 and 1.2 (GeV/c)^2 at 150, 200 and 280 GeV/c respectively.

Thus we conclude that for π^-N to $O(\alpha_s)$ QCD yields good fits to the data but it requires $\langle k_T^2 \rangle$ which increases with lab momentum of the π^-.

6. Dependence of $\langle p_T \rangle$ and $\langle p_T^2 \rangle$ on rapidity and mass of the dimuon

The dependence of the average transverse momentum squared on x_F and mass of the dimuon has been previously considered by Berger[34] and Halzen and Scott[27,35].

We have shown before (fig. 2) that $O(\alpha_s)$ QCD with K-factor indepenent of p_T and $\langle k_T^2 \rangle = 0.9$ (GeV/c)^2 is able to fit the 400 GeV/c pN data quite well. We can therefore predict the dependence of $\langle p_T \rangle$ and $\langle p_T^2 \rangle$ on rapidity for a given dimuon mass. Fig. 13 shows the predictions for M=6.5 GeV. Whereas the dependence of $\langle p_T \rangle$ on y is feeble, there is a fairly strong dependence of $\langle p_T^2 \rangle$ on y. The data of

Seattle-Michigan-Northeastern-Tufts[21] on $\langle p_T \rangle$ vs. x_F for 400 GeV/c pN agrees quite well with the above prediction. Unfortunately, there is no data on $\langle p_T^2 \rangle$ vs. y or x_F for pN reactions with which the prediction could be compared.

Fig. 14 shows the data of NA3 collaboration for $\langle p_T^2 \rangle$ vs. y, $0.25<\tau<0.37$, for π^-N reactions at 150, 200 and 280 GeV/c. Our QCD predictions are also shown in the figure. The agreement of the theory and the data is quite good.

Fig. 15 shows the data and the QCD predictions for the dependence of $\langle p_T \rangle$ on dimuon mass for pN collisions at 400 GeV/c[20] ($\langle y \rangle$=0.03), 300 GeV/c ($\langle y \rangle$=0.21), 200 GeV/c ($\langle y \rangle$=0.40) and pp collisions at $\sqrt{s}$=62 GeV[23] ($y \geq 0$). The predictions and the data are in reasonable agreement within errors.

Fig. 16 shows a comparison of the QCD predictions with the π^-N data[15] for $\langle p_T^2 \rangle$ vs. M. The two disagree rather violently.

7. Energy dependence of $\langle p_T^2 \rangle$ and $\langle p_T \rangle$

We have seen in sect. 5 that while $O(\alpha_s)$ QCD is able to fit quite well the data on p_T distribution of dimuons, the fits require a $\langle k_T^2 \rangle$ which is large and which increases as s increases. This failure of the first order QCD can be demonstrated graphically in a different manner[36].

A well known prediction[28,34,37] of perturbative QCD to $O(\alpha_s)$ for the dimuon production is that

$$\langle p_T^2 \rangle = \langle k_T^2 \rangle + \alpha_s(Q^2) \cdot f(\tau, x_F, \ln Q^2) \cdot s \qquad (7)$$

where $\langle k_T^2 \rangle$ is the non-perturbative contribution arising from the transverse momentum of the constituents taking part in the interaction. The eq. (1) implies that $\langle p_T^2 \rangle$ should increase linearly with s for a given τ and x_F. This expectation of a linear relationship has indeed been confirmed using the data available then[38,13,15]. There is now additional data available from experiment E537.

Fig. 17 shows the measurements of $\langle p_T^2 \rangle$ for $\sqrt{\tau}=0.28$ and $x_F \geq 0$ at different values of s for π^-N reaction[13-16]. Fig. 18 shows the same for pN data[13,20,23] for $\sqrt{\tau}=0.22$. The three points from CFS are for $\langle y \rangle$ ranging from 0.03 for 400 GeV/c to 0.40 for 200 GeV/c. Since the QCD predictions are able to reproduce the dependence of $\langle p_T^2 \rangle$ on y, we have used the theory to correct CFS points to correspond to $x_F \geq 0$. Linear fits of the form $\langle p_T^2 \rangle = A + Bs$ are shown in the figures for both π^-N and pN data. The details of the fits are given in table 3. The values of the intercept are equal within errors for π^-N and pN data but the slope of the increase of $\langle p_T^2 \rangle$ with s is approximately twice as large for the π^-N as for the pN data.

Since within errors the intercepts for π^-N and pN data are equal and since from eq. 7 the intercepts can be interpreted as equal to $\langle k_T^2 \rangle$, we have set $\langle k_T^2 \rangle = 0.59$ (GeV/c)^2 in the QCD

calculations. The results of the QCD calculations with this assumption and for two different choices of Λ(0.3 and 0.5 GeV/c) are shown in figs. 17 and 18. The predictions of the QCD fall well below the data in the case of pN as well as π^-N reactions. However, the calculations do show a steeper slope for π^-N than for pN in qualitative agreement with the data.

The value of $\langle k_T^2 \rangle = 0.59 \pm 0.05$ (GeV/c)^2 deduced here implies a value of $\langle k_T^2 \rangle_q = 0.30 \pm 0.03$ (GeV/c)^2 for each of the parton participating in the interation. This value is considerably larger than the value of 0.16 ± 0.01 (GeV/c)^2 which has been determined[26] for the average intrinsic transverse momentum squared of the quarks from the p_T^2 distributions of the meson resonances.

Fig. 19 and 20 show the data on the dependence of $\langle p_T \rangle$ on $\sqrt{s}$ for π^-N[13-16] and pN[13,20,23] reactions, respectively. Fits of the form $\langle p_T \rangle = A + B\sqrt{s}$ are shown for both sets of the data. The details of the fits are given in the table 3. As can be seen the linear relationship fits the data quite well.

The important conclusions of this section are: (i) $\langle p_T^2 \rangle$ of dimuons grows linearly with s in qualitative agreement with QCD, (ii) the growth of $\langle p_T^2 \rangle$ with s is much faster than predicted by $O(\alpha_s)$ QCD for any reasonable value of $\langle k_T^2 \rangle$.

8. Soft gluon effects

We have seen that $O(\alpha_s)$ QCD, even with the inclusion of $O(\alpha_s^2)$ through the assumption of a p_T independent K-factor, is unable to account for the observed transverse momentum spectra of the dimuons. The fits require $\langle k_T^2 \rangle$ which increases with s both for pN and $\pi^- N$ reactions. This may indicate that the higher order QCD diagrams and/or the contributions of the multiple soft gluons are important. The soft gluon effects are non-perturbative and are therefore difficult to calculate. Ambitious attempts are being made to calculate the soft gluon effects by C. Collins, D. Soper, W. Tung and their collaborators and M. Greco, G. Curci and P. Chiappetta, and R. Odorico (e.g. see the talks of Collins, Soper, Tung, Greco and Odorico in the proceedings of this Workshop).

Greco and his collaborators[39] have evaluated the soft gluon effects by using the so-called Double Leading Logarithmic Approximation (DLLA) which resums in each order only the dominant terms of the expansion. They keep track of the exact momentum conservation by working in the impact parameter space. With this approach they have been able to obtain reasonable fits to the data of CFS and NA3 collaborations on p_T spectra, $\langle p_T^2 \rangle$ vs. y and $\langle p_T^2 \rangle$ vs. M. They include the QCD hard term to fit the tail of the p_T distributions. An important feature of their fits is that they need a fairly low value of the intrinsic transverse momentum, $\langle k_T^2 \rangle = 0.4$ (GeV/c)^2 i.e. $\langle k_T^2 \rangle_q = 0.2$ (GeV/c)^2 which is in agreement with the results of Malhotra and Orava[26].

9. Nuclear effects

Since the cross section for dimuon production in a proton target is small, dimuon experiments are generally carried out with nuclear targets to take advantage of the expected $A^{1.0}$ dependence of the cross section. The question arises whether the use of the nuclear target could significantly affect the predictions for the dimuon cross section as well as the differential distributions. For example, one might expect that the elastic and inelastic collisions suffered by a hadron propagating through a nucleus could modify the transverse and longitudinal distributions of its constituents as well as their color quantum number correlations. Possible nuclear effects have been considered by Michael and Wilk[40], Bodwin et al.[41] and Godbole and Sarma[42].

Bodwin et al.[41] have argued that whereas quarks and gluons within the incoming hadron have no time to interact with each other during their passage through the nucleus, initial state interaction can occur between the constituents of the beam and those of the target. Such initial state interactions can modify not only the transverse momentum distribution but also the p_T integrated cross section $d\sigma/dQ^2dx_F$, because of the changes in the color wave function of the active quarks. However, the nuclear cross sections for Drell-Yan could still scale roughly as A^1 in agreement with the experimental observations. The expected increase in the p_T^2 is $\delta(p_T^2) \sim (0.2)^2 A^{1/3} \sim 0.23$ (GeV/c)^2 for a platinum target.

Michael and Wilk[40] have used a simplified approach to calculate the effect of multiple scattering and absorption. The exponent α in the A dependence is a function of M, x_F and p_T. For 400 GeV/c pA collisions (A=216), M=7.5, x_F=0, the values of α are found to be about 0.96, 1.0 and 1.07 for p_T=0, 1.2 and 4.5 GeV/c, respectively. Averaged over the p_T distribution, $\langle\alpha\rangle \simeq 1.0$. The effect is slightly stronger for a π^- beam, $\delta\langle p_T^2\rangle \simeq 0.4$ $(GeV/c)^2$ for A=216. The effect tends to saturate with A, i.e. the change with A for large nuclei is small.

There is some evidence for the increase in $\langle p_T^2\rangle$ with A from the results of CIP collaboration [43,41] who used C, Cu and W targets. However, the results of NA3 collaboration[15], presented in table 4, for $\langle p_T^2\rangle$ for π^- beams with W and proton targets at 150 and 280 GeV/c beam momenta, do not show the expected dependence of $\langle p_T^2\rangle$ on A.

Godbole and Sarma[42] have considered a somewhat different nuclear effect. They have suggested that the sea $q\bar{q}$ pairs could be enhanced in the nucleus due to the mutual interactions of the nucleons of the nucleus. The additional sea, $xS_A(x) = [(A-1)/2]\, 3.5\times10^{-3}(1-x)^{15}$, is much softer than the nucleon sea (the exponent 15 is only a rough estimate). If this is true then its effect would be to enhance the dimuon production at large x_F and small M. In particular, the exponent α in the A^α dependence would be expected to increase with x_F and decrease with M at a fixed s, and increase with s at a fixed M. Also, the effect would be more pronounced for the beams of p, π^+, K^+ compared to $\bar{p}$, π^-, K^-

respectively. As an example, for a 226 π^- beam impinging on Cu and W targets, α is expected to increase from 1.0 at $x_F \sim 0.1$ to 1.10 at $x_F \gtrsim 0.7$ (α=1.08 to 1.2 for π^+) and to decrease from 1.10 at M=4 to 0.98 at M=8 (α=1.18 to 1.05 for π^+). The expectation of an enhanced sea in the nucleus may in fact have already been seen by the EMC collaboration[44] who find that the structure functions for deep inelastic muon scattering off iron are significantly softer compared to those off deuterium target.

It is clear that a number of interesting A dependent effects are expected for the dimuon production in hadronic collisions. An important emphasis of the next generation of Drell-Yan experiments should be to look for A dependence in p_T, x_F and M at different energies and using different beams. There is a need for a careful experiment to study the dependence of $\langle p_T^2 \rangle$ on A with π^- (or π^+) as beam and hydrogen (or deuterium, perhaps even better), C and W as targets. Another useful experiment would be to look for enhanced nuclear sea by studying the A dependence for x_F using π^+ (or π^-) and p beams and above mentioned targets. Note that if the analysis is carried out assuming A^1 dependence, then one should see the effect in the K factor which would be expected to have a larger value at low mass (4-6 GeV) and also at high x_F ($\gtrsim 0.8$). These experiments would be particularly interesting with higher energy beams which would become available soon from the Tevatron-II at Fermilab.

10. Conclusions

We have comprehensively reviewed information on the transverse momentum spectra of high mass lepton pairs produced in hadronic interactions. The details of the calculations based on $O(\alpha_s)$ QCD, including $O(\alpha_s^2)$ effects through the use of a p_T independent K factor, are outlined. Sensitivity of the calculations to the parameters used is discussed. A discussion of the possible nuclear effects which can influence various features of the dimuon production with nuclear targets is included. Our main conclusions are briefly mentioned below.

1. The data on transverse momentum spectra of dimuons produced in pN, $\bar{p}N$ and π^-N reactions can be fitted quite well on the basis of QCD predictions to $O(\alpha_s)$ obtained using Altarelli et al. prescription for regularization based on a gaussian form for the intrinsic transverse momentum (k_T) of partons.
2. While the fits are good, they require a large value of $\langle k_T^2 \rangle$. Furthermore, the value of $\langle k_T^2 \rangle$ required increases with $\sqrt{s}$ from 0.9 $(GeV/c)^2$ at low $\sqrt{s}$ to 1.5 $(GeV/c)^2$ at $\sqrt{s}$=62 GeV.
3. For fixed values of $\sqrt{\tau}$, $\langle p_T^2 \rangle$ and $\langle p_T \rangle$ are found to grow linearly with s and $\sqrt{s}$, respectively, for both pN and π^-N reactions.
4. The intercepts of $\langle p_T^2 \rangle$ at s=0 are found to be $\langle k_T^2 \rangle = 0.59 \pm 0.05$ $(GeV/c)^2$ for π^-N reactions and 0.52 ± 0.11 $(GeV/c)^2$ for pN reactions. These are equal to each other within errors.

5. The slope of the rise of $\langle p_T^2 \rangle$ with s is approximately twice as large for π^-N data as for the pN data.
6. Assuming $k_T^2=0.59\pm0.05$ $(GeV/c)^2$ we have calculated QCD predictions, for π^-N and pN, for the dependence of $\langle p_T^2 \rangle$ on s for two different choices of $\Lambda=0.3$ and 0.5 GeV/c. The QCD predictions fall well beow the data with the disagreement increasing as s increases.
7. Thus, the QCD to $O(\alpha_s)$ and in some sense to $O(\alpha_s^2)$ is unable to account for the observed features of the p_T distributions in a satisfactory manner. There is therefore a need to extend the calculations to higher orders and to include soft gluon effects.
8. A striking and rather surprising feature of the data is near absence of the nuclear effects.

We conclude this talk by emphasising that there is a need for the next generation of dimuon experiments to, (a) concentrate on looking for nuclear effects in certain kinematic regions and (b) study detailed features of associated hadrons.

Acknowledgements

I am grateful to Drasko D. Jovanovic and Fermilab for hospitality. I would like to thank Marti Bennett for careful typing and Carmen Vera for drawings in this article.

REFERENCES

1. J.H. Christenson et.al., Phys. Rev. Lett. 25, 1523 (1970).

2. S.D. Drell and T.M. Yan, Phys. Rev. Lett. 25, 316 (1970).

3. L. Lyons, Oxford report OXF 80/80 (1980).

4. R. Stroynowski, Physics Reports C71 (1981).

5. G. Mathiae, Rivista del Nuevo Cimento 4 (1981).

6. E.L. Berger, Proc. of Workshop on Drell Yan Processes, Oct. 7-8, (1982).

7. L. Lederman, Proc. of 19th Int. Conf. on High Energy Physics, Tokyo, 706 (1978).

8. J. Pilcher, Proc. of Int. Symposium on Lepton and Photon Interactions at High Energies 185 (1979).

9. J. Lefrancois, Proc. of the XX Int. Conf. on High Energy Physics, Madison, (1980).

10. A. Michelini, Proc. of EPS Int. Conf. on High Energy Physics, Lisbon, (1981) (CERN-EP 81-128).

11. B. Cox, Proc. of XXI Int. Conf. on High Energy Physics, Paris, (1982).

12. C. Reece et al., Phys. Lett. 85B, 427 (1979); D. McCal et al., Phys. Lett. 85B, 432 (1979).

13. M. Corden et al., Phys. Lett. 96B, 417 (1980); ibid., Paper submitted to EPS Conf. on High Energy Physics, Lisbon (1981).

14. E. Anassontzis et al., Athens-Fermilab-McGill - Michigan - Shandong Collaboration, FERMILAB-CONF-82/50-EXP (1982).

15. J. Badier et al., Phys. Lett. 89B, 145 (1979); CERN/EP 80-148 (1980); Phys. Lett. 93B, 354 (1980); Phys. Lett. 96B, 422 (1980); Z. Phys. C11, 195 (1981); Phys. Lett. 104B, 335 (1981); LPNHE/X83/02 (1982); S. Weisz, Talk at the Workshop on Drell-Yan Processes, Fermilab (1982).

16. K.J. Anderson et al., Phys. Rev. Lett. 42, 944, (1979); Phys. Rev. Lett. 42,948(1979); Phys. Rev. Lett. 42,951 (1979).

17. B. Louis, Workshop on Drell-Yan Processes, Fermilab (1982).

18. D. Stickland, Workshop on Drell-Yan Processes, Fermilab (1982).

19. S. Falciano et al., CERN-EP/81-52 (1981); H. Suter and V. Telegdi, Workshop on Drell-Yan Processes, Fermilab (1982).

20. A.S. Ito et al., Phys. Rev. D23, 604 (1981).

21. S.R. Smith et al., Phys. Rev. Lett. 46, 1607 (1981).

22. S.R. Smith et al., Workshop on Drell-Yan Processes, Fermilab (1982).

23. D. Antreasyan et al., Phys. Rev. Lett. 45, 863 (1980); 47, 12 (1981); 48, 302 (1982).

24. The author thanks Dr. M. Chen and Dr. U. Becker for sending unpublished data on p_T distribution at $\sqrt{s}$=44 GeV and Dr. D. Antreasyan for discussion on the data.

25. R.D. Field, Lectures given at the Boulder Summer School on Quantum Flavordynamics, QCD and Unified Theories, CALT-68-739 (1979).

26. P.K. Malhotra and R. Orava, A determination of intrinsic transverse momentum of quarks, FERMILAB-Pub-82/80 (1982).

27. F. Halzen and D.M. Scott, Phys. Rev. D18, 3378 (1978), K. Kajantie and R. Raitio, Nucl. Phys. B139, 72 (1978).

28. G. Altarelli, G. Parisi and R. Petronzio, Phys. Lett. 76B, 351 (1978); Phys. Lett. 76B, 356 (1978).

29. G. Altarelli, R.K. Ellis and G. Martinelli, Nucl. Phys. B157, 461 (1979); J. Kubar-Andre and F.E. Paige, Phys. Rev. D19, 221 (1979); J. Kubar et al., Nucl. Phys. B175, 251 (1980).

30. R.K. Ellis, G. Martinelli and R. Petronzio, Phys. Lett. 104B, 45 (1981).

31. F. Eisele, Structure Functions, Review talk given at XXI Int. Conf. on High Energy Physics, Paris (1982).

32. J.G.H. deGroot et al., Z. Physic C1, 143 (1979) and Phys. Lett. 82B, 456 (1979).

33. B. Cox, Proc. of the Workshop on Drell-Yan Processes, Fermilab (1982).

34. E.L. Berger, AIP Conf. Proc. No. 45, Vanderbilt, Ed. by R. Panvini and S.E. Csorna (1978); ibid. Proc. of the Int. Meeting on Frontiers of Physics, Singapore, Ed. by K.K. Phua (1978); High Energy Physics in the Einstein

Centennial Year, Ed. by A. Perlmutter et al., (N.Y. Plenum Press, 1979).

35. F. Halzen and D.M. Scott, Phys. Rev. D19, 216 (1979).

36. B. Cox and P.K. Malhotra, Submitted for publication (1982).

37. F. Halzen and D.M. Scott, Proc. of Moriond Workshop on Lepton Pair Production, Ed. by J. Tran Thanh Van, 297 (1981).

38. J.K. Yoh et al., Phys. Rev. Lett. 41, 684 (1978).

39. G. Curci and M. Greco, Phys. Lett. 92B, 175 (1980); ibid., Phys. Lett. 102B, 280 (1981); P. Chiappetta and M. Greco, Phys. Lett. 106B, 219 (1981); ibid., Preprint CPT-81/p.1335; M. Greco, Proc. of the Moriond Workshop, 255 (1982).

40. C. Michael and G. Wilk, Z. Phys. C10, 169 (1981).

41. G.T. Bodwin, S.J. Brodsky and G. Peter Lapage, Phys. Rev. Lett. 47, 1799 (1981); ibid. SLAC-PUB-2860 (1981); SLAC-PUB-2927 (1982); SLAC-PUB-2966 (1982).

42. R.M. Godbole and K.V.L. Sarma, Phys. Rev. D25, 120 (1982).

43. G.E. Hogan, Ph.D. Dissertation, Princeton University (1979).

44. J.J. Aubert et al., EMC Collaboration, presented at the XXI Int. Conf. on High Energy Physics, Paris, July 1982.

Table 1. Current and recent lepton pair experiments.

Collaboration	Experiment Reference	Reaction	P_{lab} GeV/c	No. of events	Mass GeV	x_F or y
Rochester-Brookhaven-Washington	RBW(12)	$\pi^{\pm}$ Cu	16,22	-	< 4	$x_F > -0.2$
Birmingham-CERN-Ecole Poly.	BCE(Ω)(13)	$(\pi^{\pm},K^{\pm},p^{\pm})$W	39.5	3582(2<M<2.7) 257(M 4)	2-7	$x_F > 0$
Athens-Fermilab-McGill-Michigan-Shandong	E537(14)	π^- W	125	1257	4-8.5	$x_F > 0$
Saclay-CERN-CdeF-Ecole Poly.-Orsay	NA3(15)	π^-Pt	150	22000	4.1-8.5	y> -0.6
		π^+Pt	200	5600	4.1-8.5	y> -0.6
		π^-Pt	200	2000	4.1-8.5	y> -0.6
		$\pi^{\pm}$Pt	280	19000	4.1-8.5	y> -0.6
		π^-p	150,280	549,706	4.1-8.5	y> -0.6
Chicago-Illinois-Princeton	CIP(16)	$(\pi^{\pm},p^{\pm})$C,Cu,W	225	-	2-11	$x_F > 0$
Chicago-Fermilab-Iowa State-Princeton	E615(17)	π^-	225	-	≥ 4	High x_F
Chicago-Princeton	E326(18)	π^-	225	-	High Mass	-
CERN-Ecole Poly-Strasbourg-Zurich	NA10(19)	π^-C,Cu,W	280	-	4-15	$x_F > 0$
Athens-Fermilab-McGill-Michigan-Shandong	E537(14)	$\bar{p}$ W	125	416	4-8.5	$x_F > 0$
SCCEO	NA3 (15)	$\bar{p}$ Pt	150	275	4.1-8.5	$x_F > 0$
SCCEO	NA3 (15)	p Pt	200	1300	4.1-8.5	y> -0.6
Columbia-Fermilab-Stony Brook	E288(20)	pBe,Cu,Pt	200	-	4-15	0.2<y<0.6
			300	-	4-15	0<y<0.4
			400	-	4-15	-.2<y<.2
Seattle-Michigan-Northeastern-Tufts	E439(21)	pW	400	2.10^5	4-16	$-.2<x_F<.9$
CERN-Columbia-Fermilab-KEK-Kyoto-Saclay-Stony Brook-Seattle	E605(22)	$(p,\bar{\pi}^{\pm})$Be,Cu,W	>400	-	M>6	$x_F > -.1$
CERN-MIT-Annecy-Harvard-Florida-Naples-Pisa	R209(23)	pp	$\sqrt{s}$ = 44	336	5-17	$x_F > 0$
		pp	$\sqrt{s}$ = 62	1836	5-25	$x_F > 0$

Table 2. Compilation of measurements of the K-factor.

P_{lab} (GeV/c)	Reaction	K	Reference
39.5	$\pi^{\pm}N$	2.6±0.5	13
125	$\pi^{-}N$	2.5±0.5	14
150,200	$\pi^{-}N$	2.2±0.3	15
150	$\pi^{+}N$	2.4±0.4	15
150	$(\pi^{-}-\pi^{+})N$	2.2±0.4	15
150	$\pi^{-}p$	2.4±0.4	15
125	$\bar{p}N$	2.3±0.5	14
150	$\bar{p}N$	2.3±0.4	15
200	pN	2.2±0.4	15
400	pN	1.7	20
400	pN	1.6±0.3	21
2050	pp	1.6(1.8,our fit)	23

Table 3. The results of the fits of the type $\langle p_T^2 \rangle = A + B(\tau)s$ and $\langle p_T \rangle = A' + B'(\tau)\sqrt{s}$ to the data.

Fit	Reaction	$\sqrt{\tau}$	Intercept	Slope	X^2/NDF
$\langle p_T^2 \rangle$	π^-N	0.28	0.59±0.05	$(2.8\pm0.2)10^{-3}$	1.2
	pN	0.22	0.52±0.11	$(1.4\pm0.2)^{10^{-3}}$	0.3
$\langle p_T \rangle$	π^-N	0.28	0.48±0.05	$(3.4\pm0.3)10^{-2}$	0.1
	pN	0.22	0.46±0.07	$(2.5\pm0.3)10^{-2}$	0.4

Table 4. NA3 results for $\langle p_T^2 \rangle$ for π^- beam with W and proton targets at 150 and 280 GeV/c beam momenta.

Reaction	$\langle p_T^2 \rangle$ $(GeV/c)^2$	
	150 GeV/c	280 GeV/c
π^-W	1.44±0.02	1.80±0.03
π^-p	1.55±0.13	1.73±0.13

FIGURE CAPTIONS

Fig. 1. (a) Drell-Yan process $q\bar{q}\to\gamma\to\mu^+\mu^-$, where γ is the virtual photon. (b) QCD annihilation process $q\bar{q}\to g\gamma$. (c) QCD Compton process $qg\to q\gamma$. (d) vertex connection $q\bar{q}\to\gamma$, involving a virtual gluon.

Fig. 2. Summary of the theoretical calculations[29,39] for the K factor.

Fig. 3. Transverse momentum distribution of muon pairs produced in p-Pt collisions at 400 Gev/c for y=0.03 and mass equal to (a) 5-6 and 7-8 GeV, (b) 6-7 and 8-9 GeV and (c) 11-12 GeV. The data are from CFS collaboration[20]. Our fits based on $O(\alpha_s)$ QCD, described in the text, are also shown.

Fig. 4. Transverse momentum distributions of dimuons for $pp\to\mu^+\mu^-x$ at $\sqrt{s}$=62 GeV and 44 GeV from MLHNP collaboration[23,24]. Simple exponential fits shown are due to the authors.

Fig. 5. Data as in Fig. 3. The curves are $O(\alpha_s)$ QCD fits with K=1.8 and $\langle k_T^2\rangle$=1.5 $(GeV/c)^2$.

Fig. 6. Contributions of the different terms to the p_T distribution of the dimuons in pN collisions at 400 GeV/c for M=7.5 GeV and y=0.03. Sensitivity to the Λ parameter is also shown.

Fig. 7. Sensitivity to the $\langle k_T^2\rangle$ parameter for 400 GeV/c pN collisions, M=7.5 GeV, y=0.03, Λ=0.5 GeV/c.

Fig. 8. Dimuon p_T distribution in $\bar{p}W\to\mu^+\mu^-X$ reaction at 125 GeV/c, 4.0<M<8.5 GeV, y>0 from E537 collaboration[14]. The solid line shows the QCD fit with K=2.25 and $\langle k_T^2\rangle$=0.88 $(GeV/c)^2$. Contributions of different terms are also shown.

Fig. 9. Same as in Fig. 7 but for $\pi^-W\to\mu^+\mu^-x$ reactions at 125 GeV/c from E537 collaboration[14]. The value of K factor is 2.5±0.5.

Fig. 10. New plots from the NA3 collaboration[15] for $\pi^-Pt\to\mu^+\mu^-X$ at 150, 200 and 280 GeV/c.

Fig. 11. Dimuon p_T distribution in $\pi^-Pt\to\mu^+\mu^-X$ reaction at 150 GeV/c, y>-0.6 for M=4.1-500 GeV, 5-6 GeV and 4.1-8.5 GeV from NA3 collaboration[15]. Our QCD fits with K=2.3 and $\langle k_T^2\rangle$=1.0 $(GeV/c)^2$ are also shown.

Fig. 12. Dimuon p_T distribution in $\pi^-Pt\to\mu^+\mu^-X$ reactions at 150, 200 and 280 GeV/c, 4.1<M<8.5 GeV and y>-0.6 from NA3 collaboration[15]. The curves show QCD fits carried out by us with K=2.3 and $\langle k_T^2\rangle$=1.0, 1.1 and 1.2 $(GeV/c)^2$ for 150, 200 and 280 GeV/c respectively.

Fig. 13. Predictions for the dependence of $\langle p_T \rangle$ and $\langle p_T^2 \rangle$ on y based on our QCD fits to the 400 GeV/c pN data[20] for M=6.5 GeV.

Fig. 14. NA3 data for the dependence of $\langle p_T^2 \rangle$ on y, $0.25<\tau<0.37$, for π^-N reactions at 150, 200 and 280 GeV/c. The curves shown are predictions based on our QCD fits.

Fig. 15. $\langle p_T \rangle$ vs. M for pN collisions at 200, 300 and 400 GeV/c[20] and pp collisions at $\sqrt{s}=62$ GeV[23]. Predictions based on our QCD fits are also shown.

Fig. 16. $\langle p_T^2 \rangle$ vs. M for π^-N collisions at 150, 200 and 280 GeV/c[15]. The curves are predictions based on our QCD fits.

Fig. 17. $\langle p_T^2 \rangle$ vs. s for π^-N reactions[13-16] for $\sqrt{\tau}=0.28$ and $x_F \geq 0$. The solid line shows our linear fit (see table 3 for fitted parameters). Also shown are QCD predictions obtained using $\langle k_T^2 \rangle = 0.59$ (Gev/c)^2.

Fig. 18. $\langle p_T^2 \rangle$ vs. s for pN reactions[13,20,23] for $\sqrt{\tau}=0.22$ and $x_F \geq 0$. The crosses give the CFS[20] points corrected for the fact that their data corresponds to $y \leq 0.4$. The solid line shows our linear fit (see table 3). QCD predictions obtained using $\langle k_T^2 \rangle = 0.59$ (GeV/c)^2 are also shown.

Fig. 19. $\langle p_T \rangle$ vs. $\sqrt{s}$ for π^-N data[13-16] for $\sqrt{\tau}=0.28$. The curve shows our linear fit (see table 3).

Fig. 20. $\langle p_T \rangle$ vs. s for pN data[13,20,23] for $\sqrt{\tau}=0.22$. The curve shows our linear fit (see table 3).

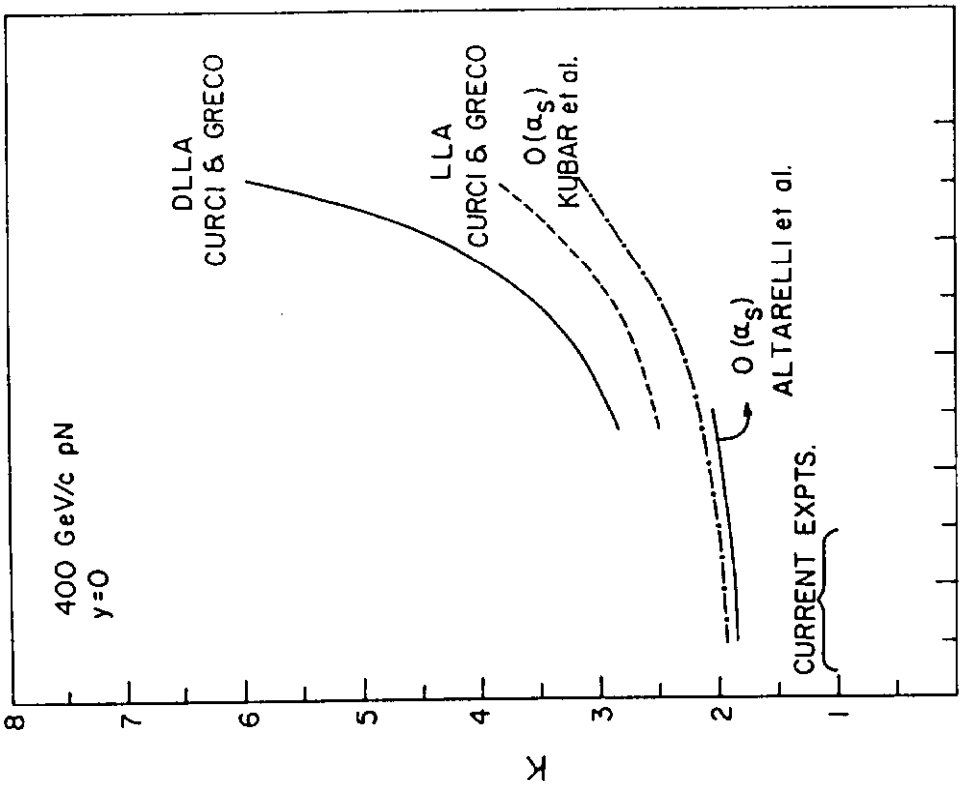
400 GeV/c pN
y=0
DLLA
CURCI & GRECO
LLA
CURCI & GRECO
O(α_S)
KUBAR et al.
O(α_S)
ALTARELLI et al.
CURRENT EXPTS.
K
τ=M²/s
0
0.2
0.4
0.6
0.8
1.0
1
2
3
4
5
6
7
8

Fig. 2

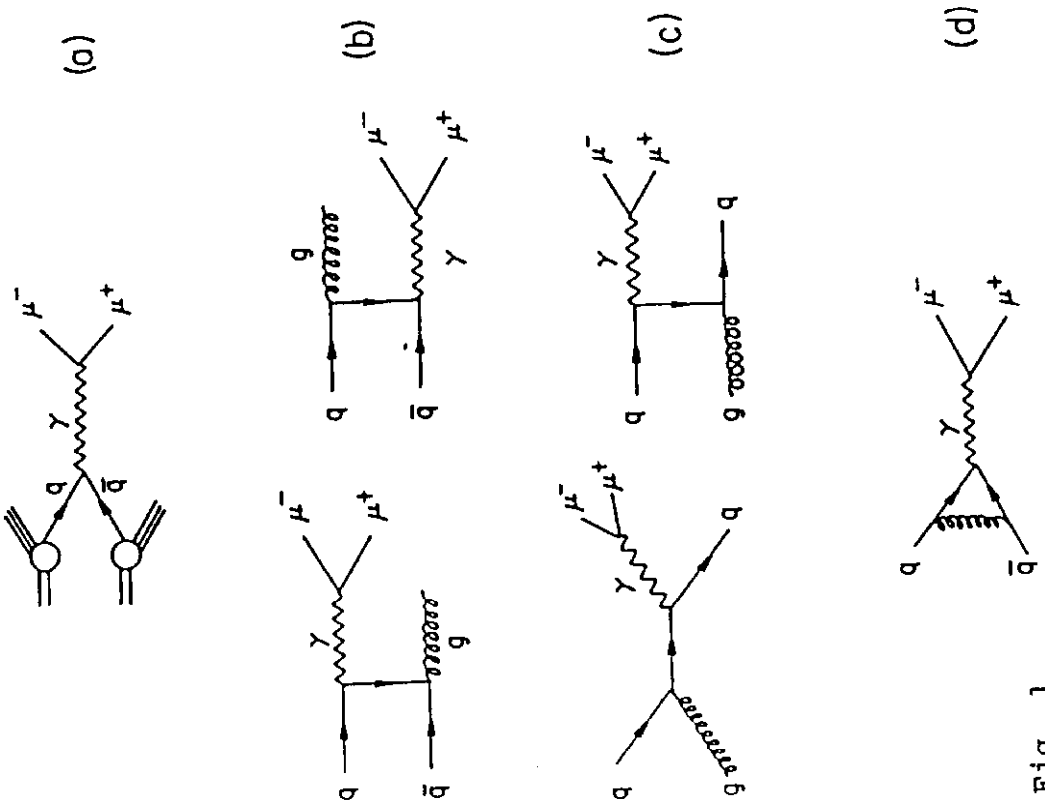
(a)
(b)
(c)
(d)
μ⁻
μ⁺
γ
q
q̄
g

Fig. 1

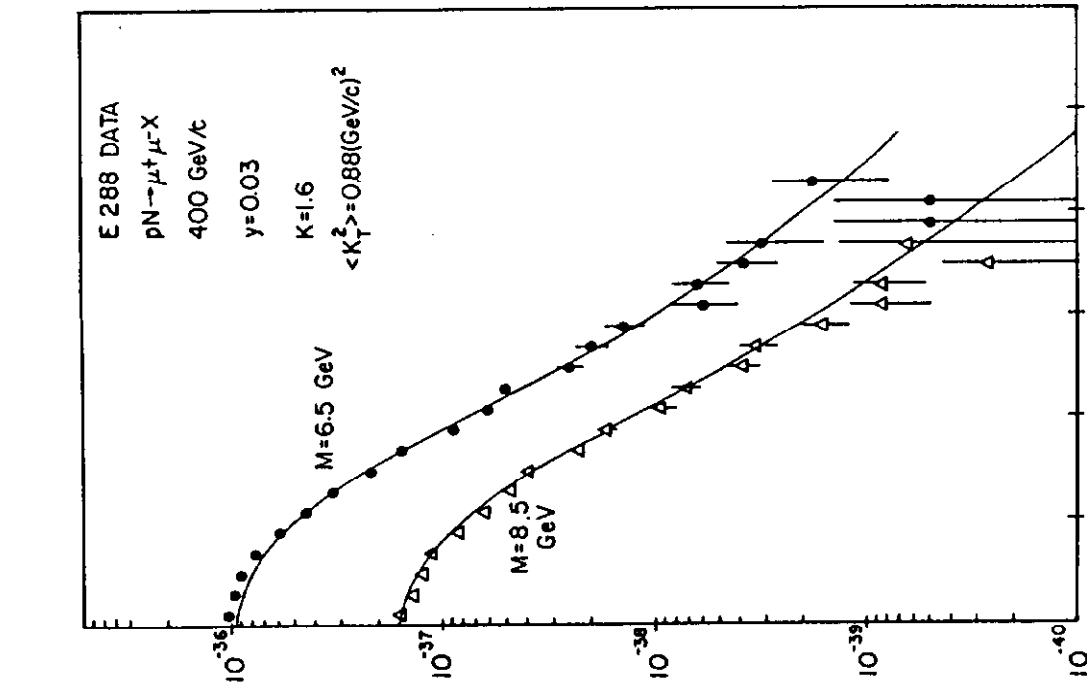
E 288 DATA
pN→μ⁺μ⁻X
400 GeV/c
y=0.03
K=1.6
<K_T^2>=0.88(GeV/c)^2
M=6.5 GeV
M=8.5 GeV
(E.d³σ/dMdP³) cm²(GeV/c)⁻³/nucleon
P_T (GeV/c)

Fig. 3 (b)

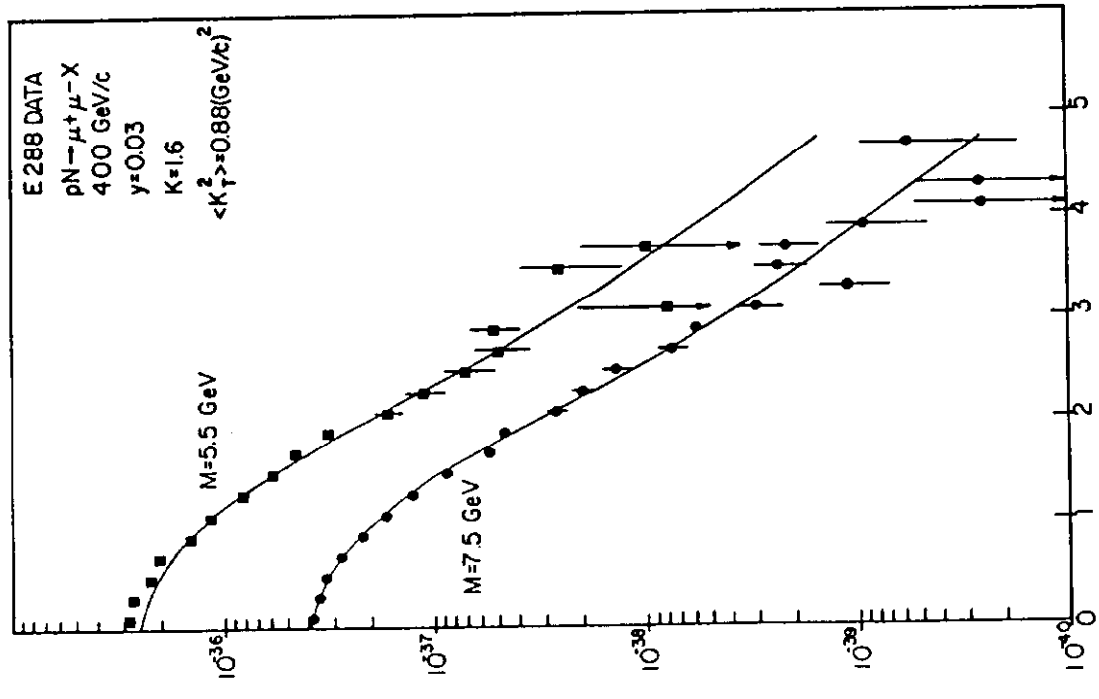
E 288 DATA
pN→μ⁺μ⁻X
400 GeV/c
y=0.03
K=1.6
<K_T^2>=0.88(GeV/c)^2
M=5.5 GeV
M=7.5 GeV
(E.d³σ/dMdP³) cm²(GeV/c)⁻³/nucleon
P_T (GeV/c)

Fig. 3 (a)

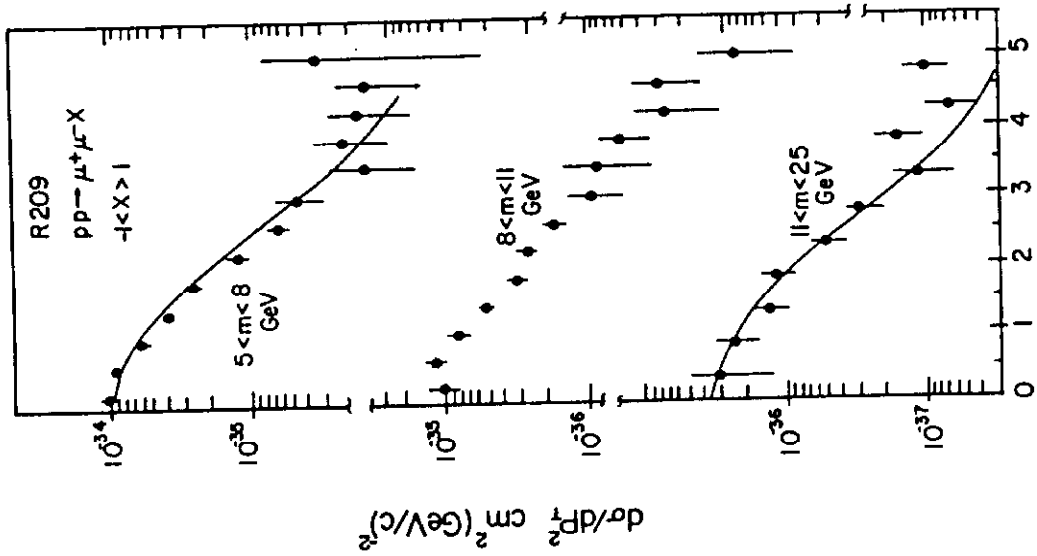
R209
pp→μ⁺μ⁻X
-1<X>1
5<m<8 GeV
8<m<11 GeV
11<m<25 GeV
dσ/dP²T cm²(GeV/c)²
PT (GeV/c)

Fig. 5

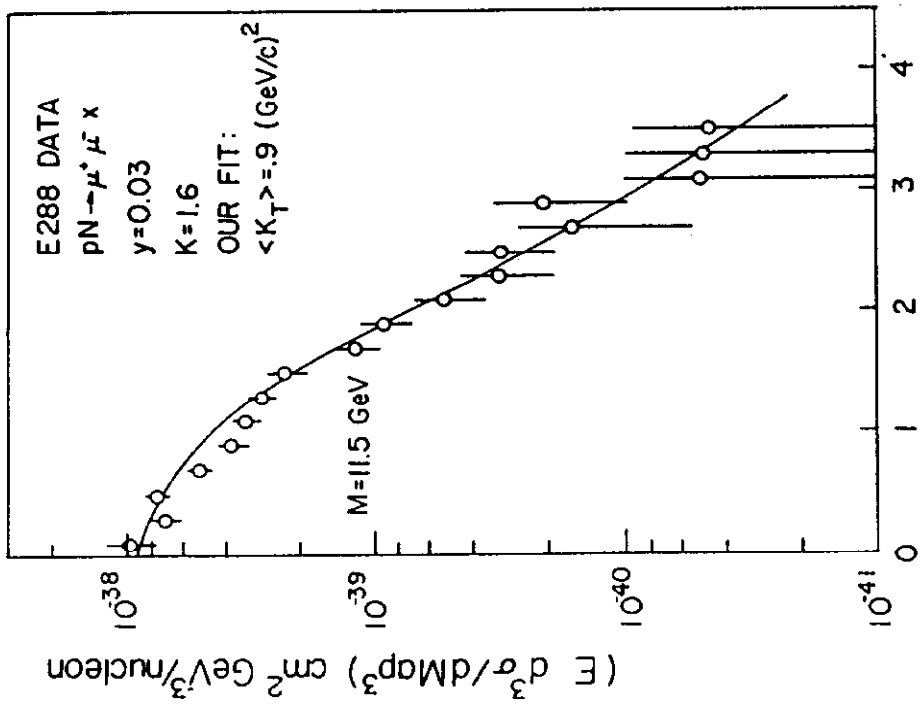
E288 DATA
pN→μ⁺μ⁻x
y=0.03
K=1.6
OUR FIT:
<KT>=.9 (GeV/c)²
M=11.5 GeV
(E d³σ/dMdp³) cm² GeV⁻³/nucleon
PT (GeV/c)

Fig. 3(c)

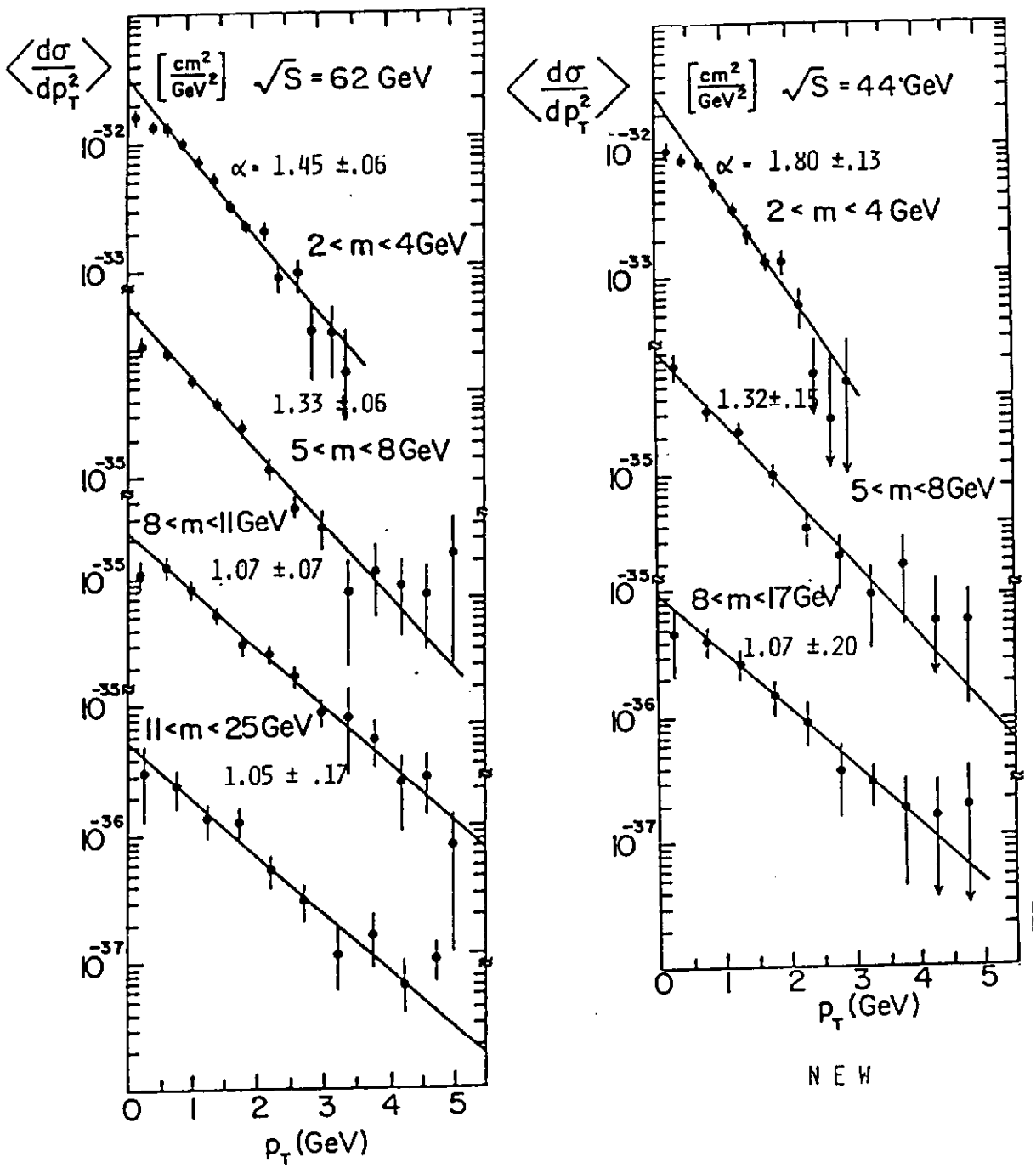

P_T - DISTRIBUTIONS AND FIT TO EXP($-\alpha P_T$) FOR $|P_T| > 0.5$ GEV.

Fig. 4

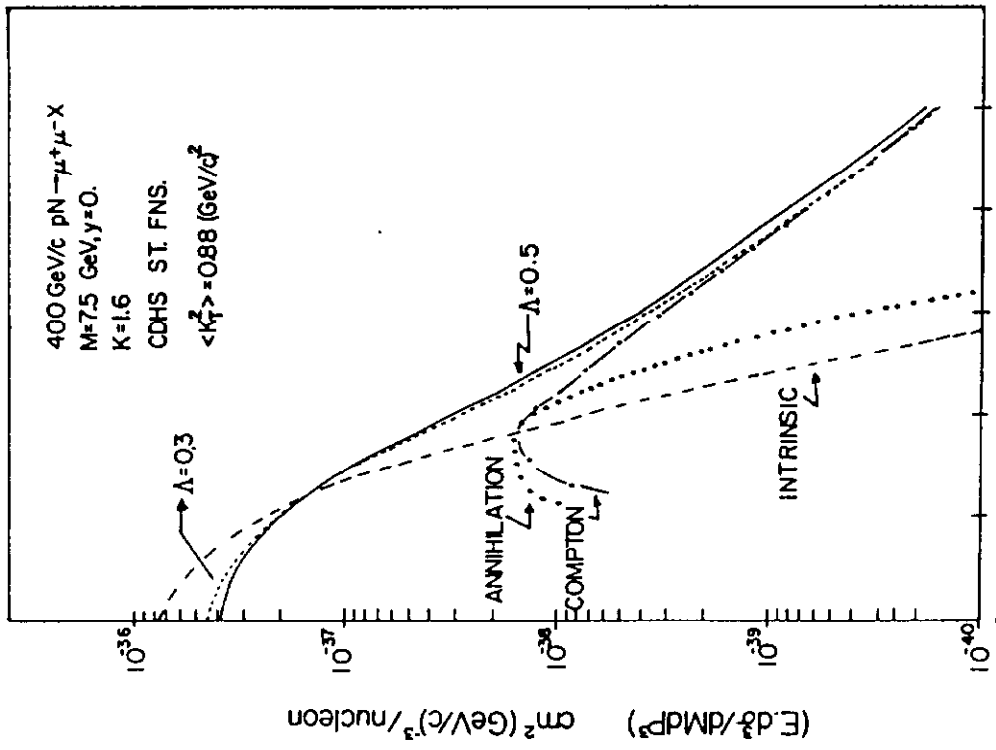
400 GeV/c pN→μ⁺μ⁻X
M=7.5 GeV, y=0.
K=1.6
CDHS ST. FNS.
<K_T²>=0.88 (GeV/c)²
Λ=0.3
Λ=0.5
ANNIHILATION
COMPTON
INTRINSIC
(E.d³σ/dMdp³) cm² (GeV/c)⁻³/nucleon
P_T (GeV/c)

Fig. 6

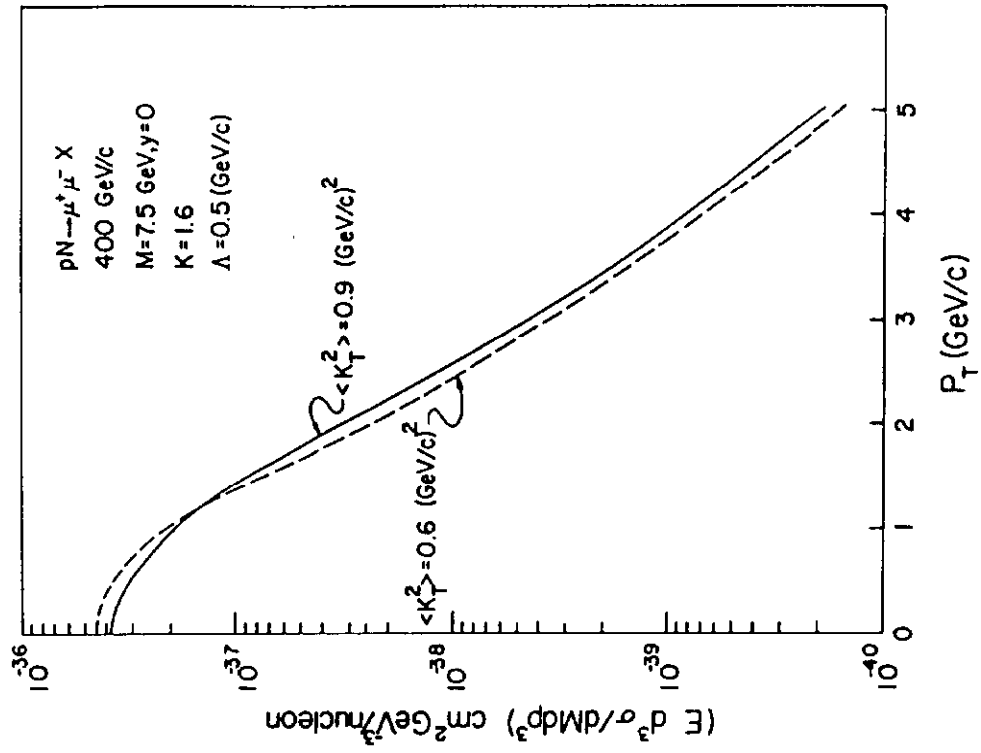
pN→μ⁺μ⁻X
400 GeV/c
M=7.5 GeV, y=0
K=1.6
Λ=0.5 (GeV/c)
<K_T²>=0.9 (GeV/c)²
<K_T²>=0.6 (GeV/c)²
(E d³σ/dMdp³) cm²GeV⁻²/nucleon
P_T (GeV/c)

Fig. 7

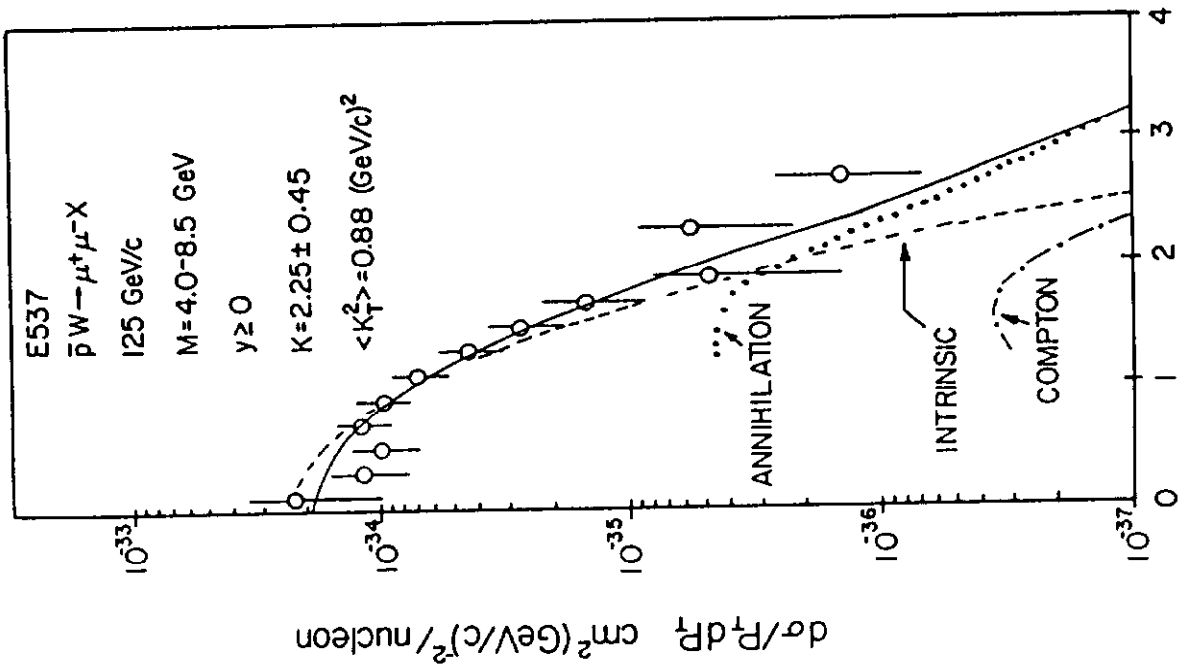
E537
$\bar{p}W \rightarrow \mu^+\mu^- X$
125 GeV/c
M=4.0-8.5 GeV
y≥0
K=2.25±0.45
$\langle K_T^2 \rangle$=0.88 (GeV/c)^2
ANNIHILATION
INTRINSIC
COMPTON
$d\sigma/P_T dP_T$ cm^2(GeV/c)$^{-2}$/nucleon
P_T (GeV/c)

Fig. 8

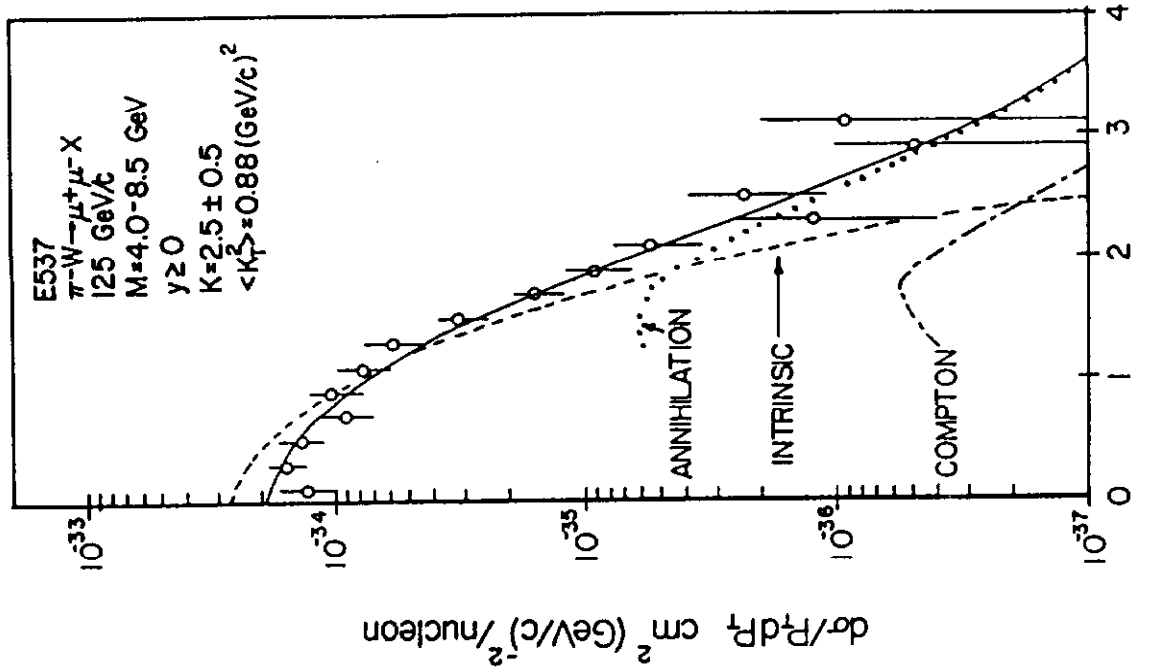
E537
$\pi^- W \rightarrow \mu^+\mu^- X$
125 GeV/c
M=4.0-8.5 GeV
y≥0
K=2.5±0.5
$\langle K_T^2 \rangle$=0.88 (GeV/c)^2
ANNIHILATION
INTRINSIC
COMPTON
$d\sigma/P_T dP_T$ cm^2 (GeV/c)$^{-2}$/nucleon
P_T (GeV/c)

Fig. 9

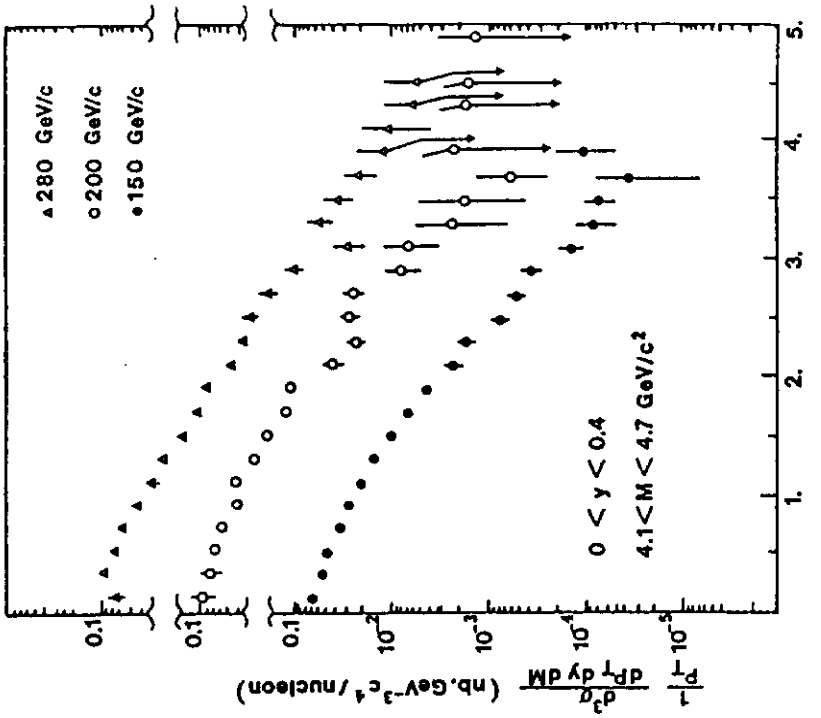

Fig. 10(b)

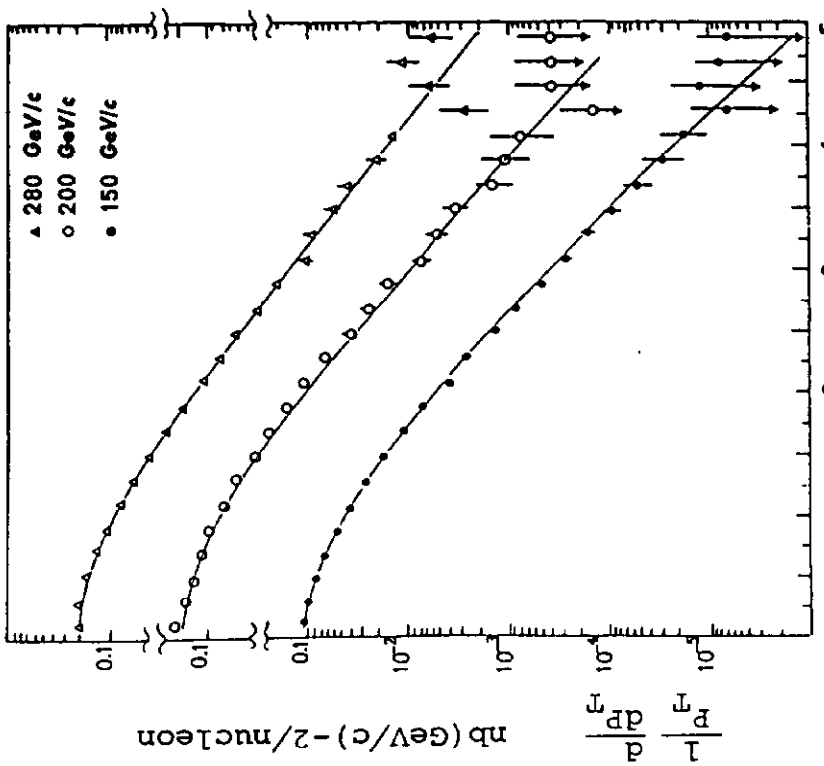

Fig. 10(a)

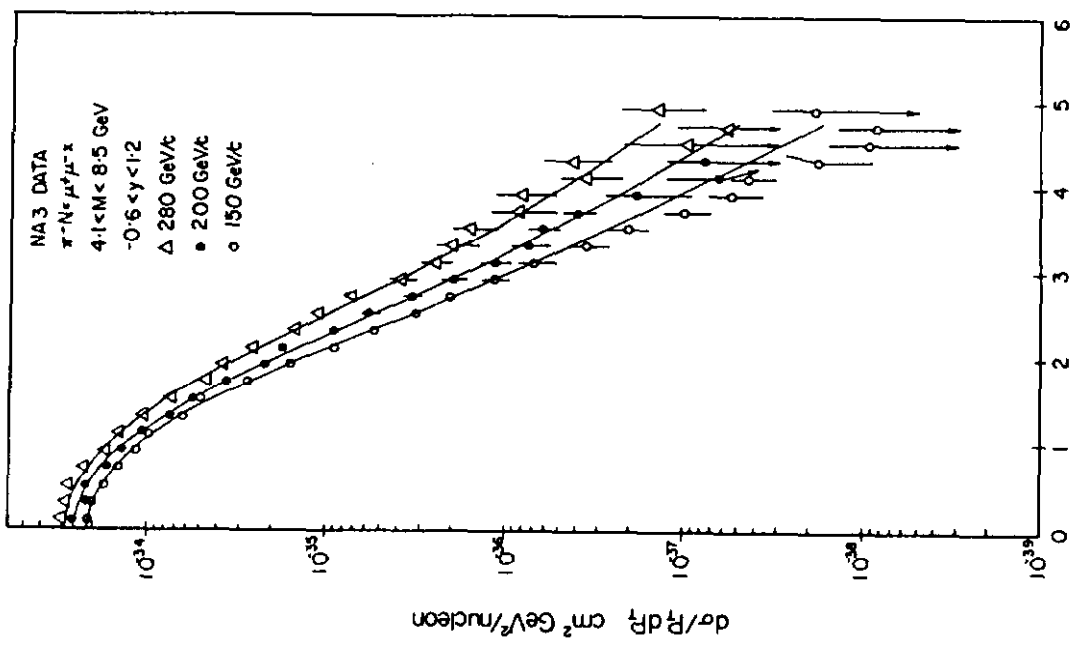
NA3 DATA
π⁻N→μ⁺μ⁻x
4·1<M<8·5 GeV
-0·6<y<1·2
△ 280 GeV/c
• 200 GeV/c
○ 150 GeV/c
dσ/R dR_T cm² GeV²/nucleon
R_T (GeV/c)

Fig. 12

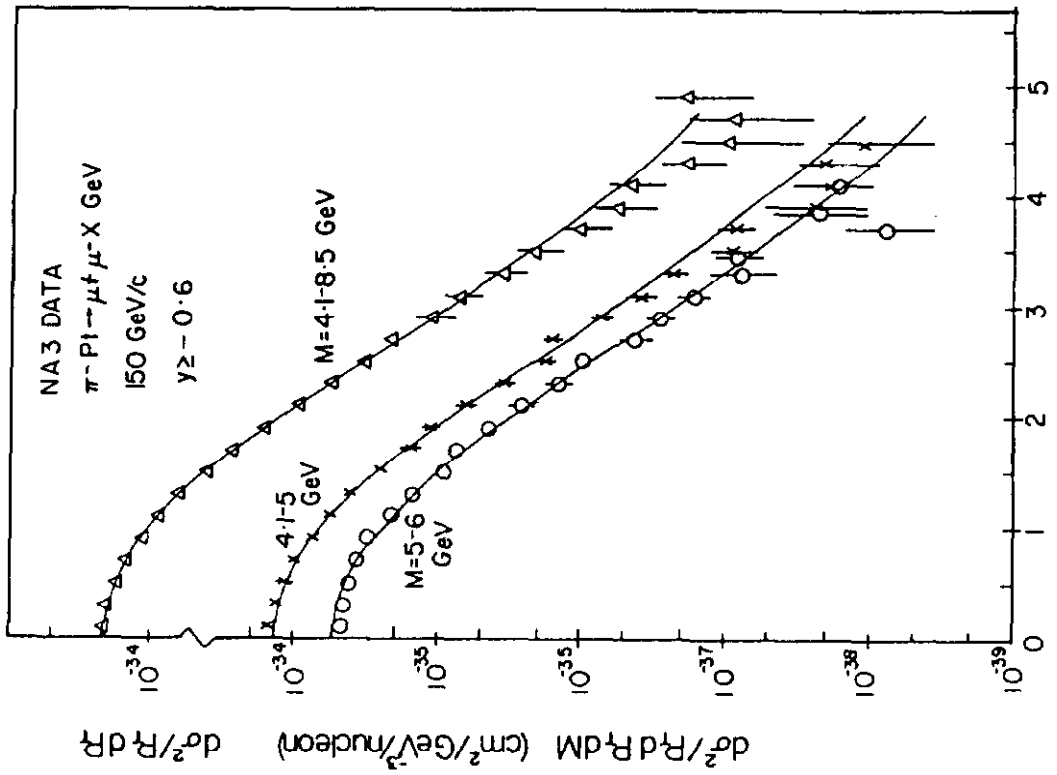
NA3 DATA
π⁻ Pt → μ⁺μ⁻X GeV
150 GeV/c
y≥-0·6
M=4·1-8·5 GeV
4·1-5 GeV
M=5-6 GeV
d²σ/R dR_T dM (cm²/GeV⁻³/nucleon)
d²σ/R dR_T
R_T (GeV/c)

Fig. 11

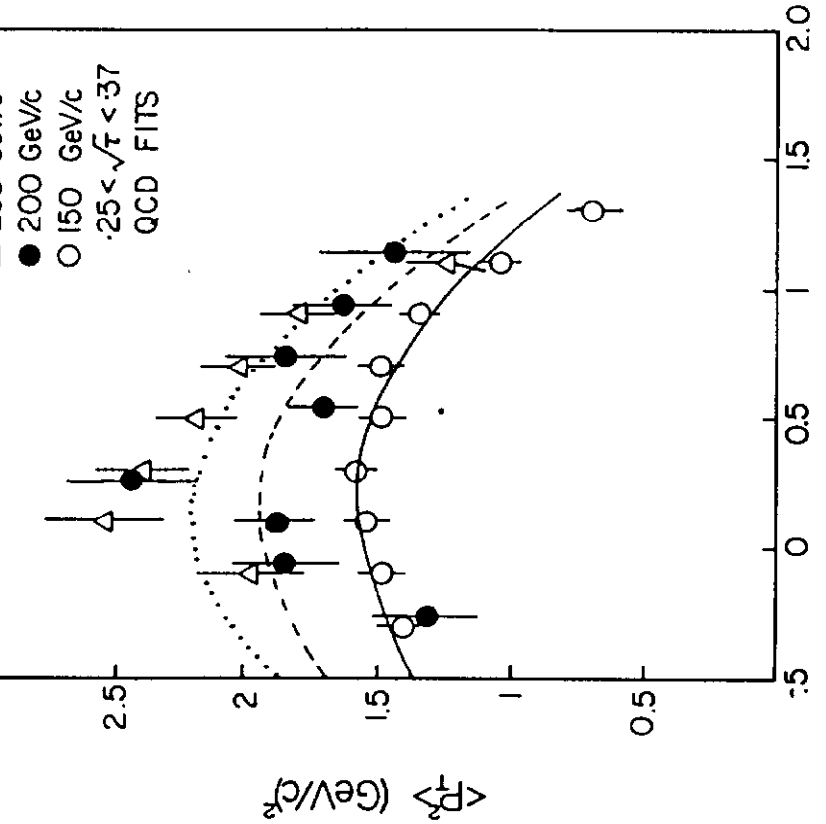
NA3 DATA
△ 280 GeV/c
● 200 GeV/c
○ 150 GeV/c
.25<√τ<.37
QCD FITS
<p_T^2> (GeV/c)^2
y

Fig. 14

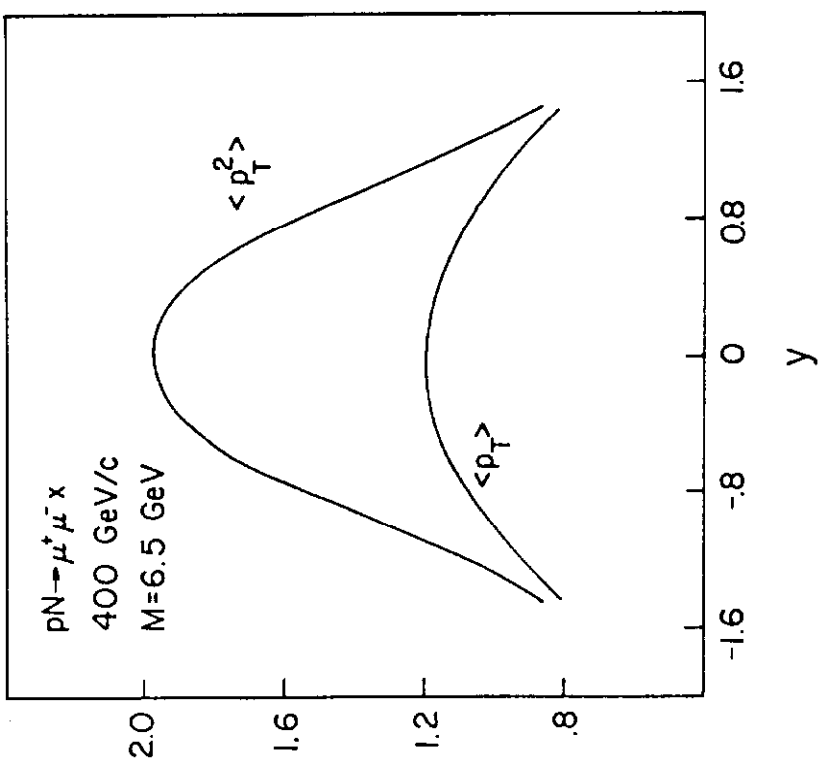
pN→μ⁺μ⁻X
400 GeV/c
M=6.5 GeV
<p_T^2>
<p_T>
y

Fig. 13

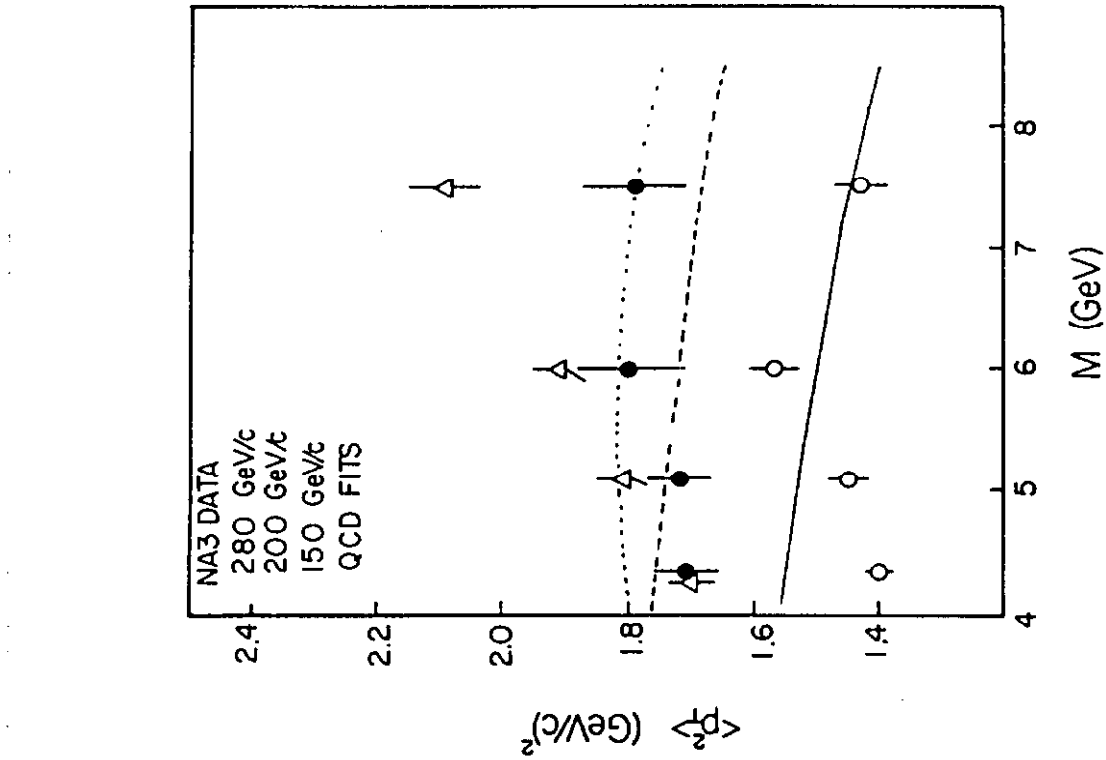
NA3 DATA
280 GeV/c
200 GeV/c
150 GeV/c
QCD FITS
<p_T^2> (GeV/c)^2
M (GeV)

Fig. 16

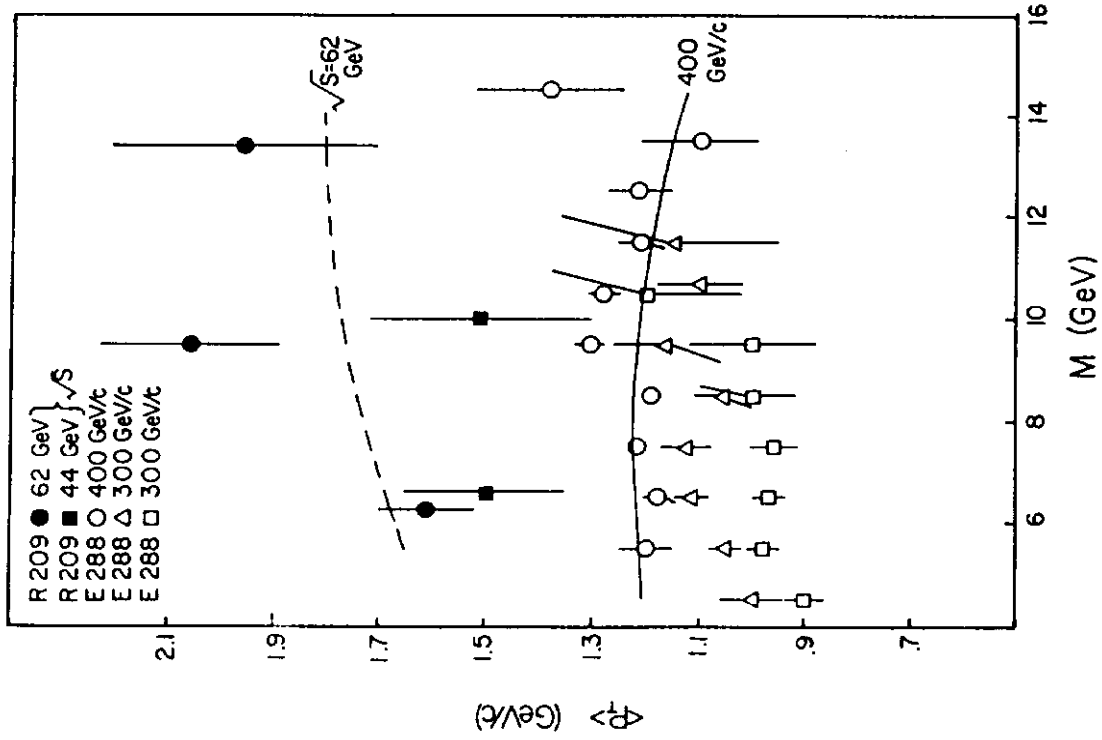
R 209 ● 62 GeV
R 209 ■ 44 GeV
E 288 ○ 400 GeV/c
E 288 △ 300 GeV/c
E 288 □ 300 GeV/c
√S
√S=62 GeV
400 GeV/c
<p_T> (GeV/c)
M (GeV)

Fig. 15

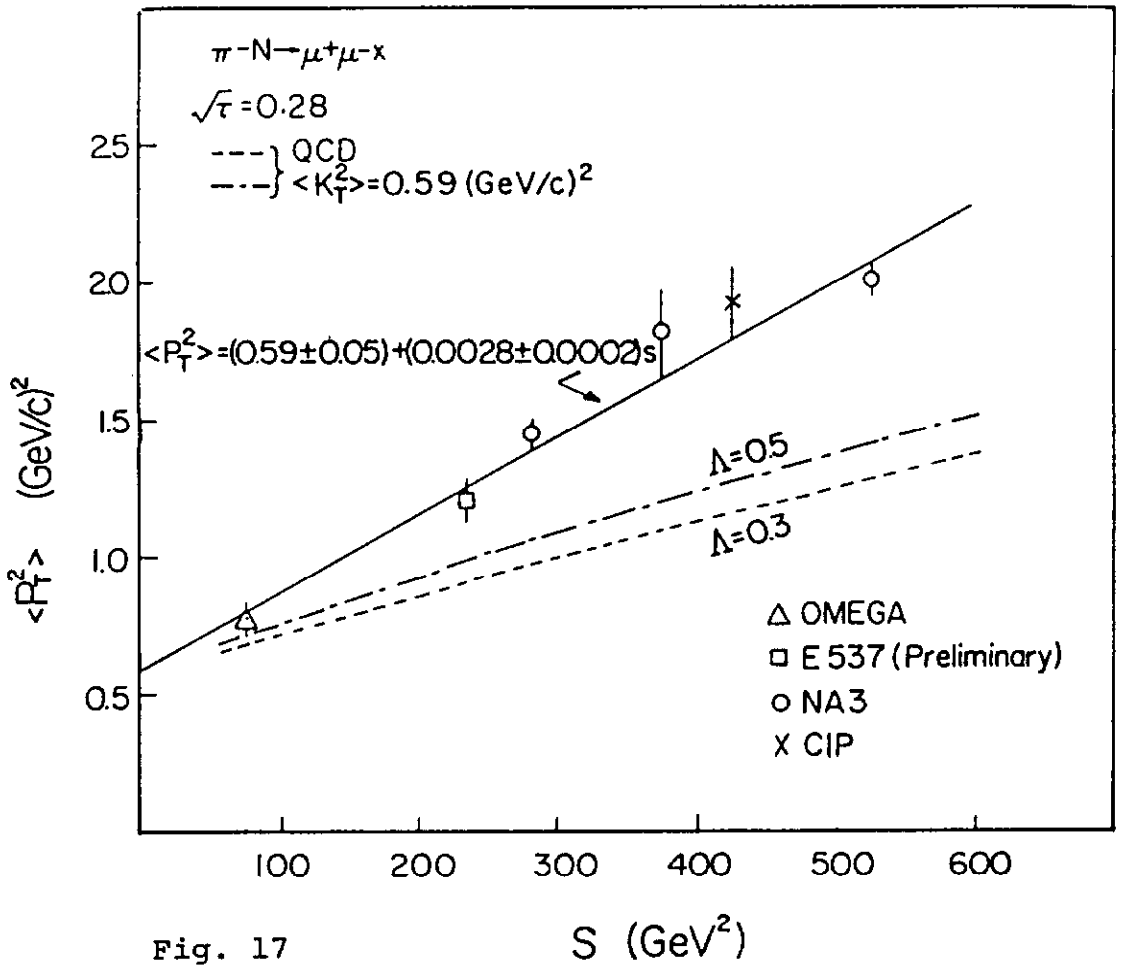
π⁻N→μ⁺μ⁻X
√τ=0.28
QCD
<K_T²>=0.59 (GeV/c)²
<P_T²>=(0.59±0.05)+(0.0028±0.0002)s
Λ=0.5
Λ=0.3
△ OMEGA
□ E 537 (Preliminary)
○ NA3
X CIP
<P_T²> (GeV/c)²
S (GeV²)

Fig. 17

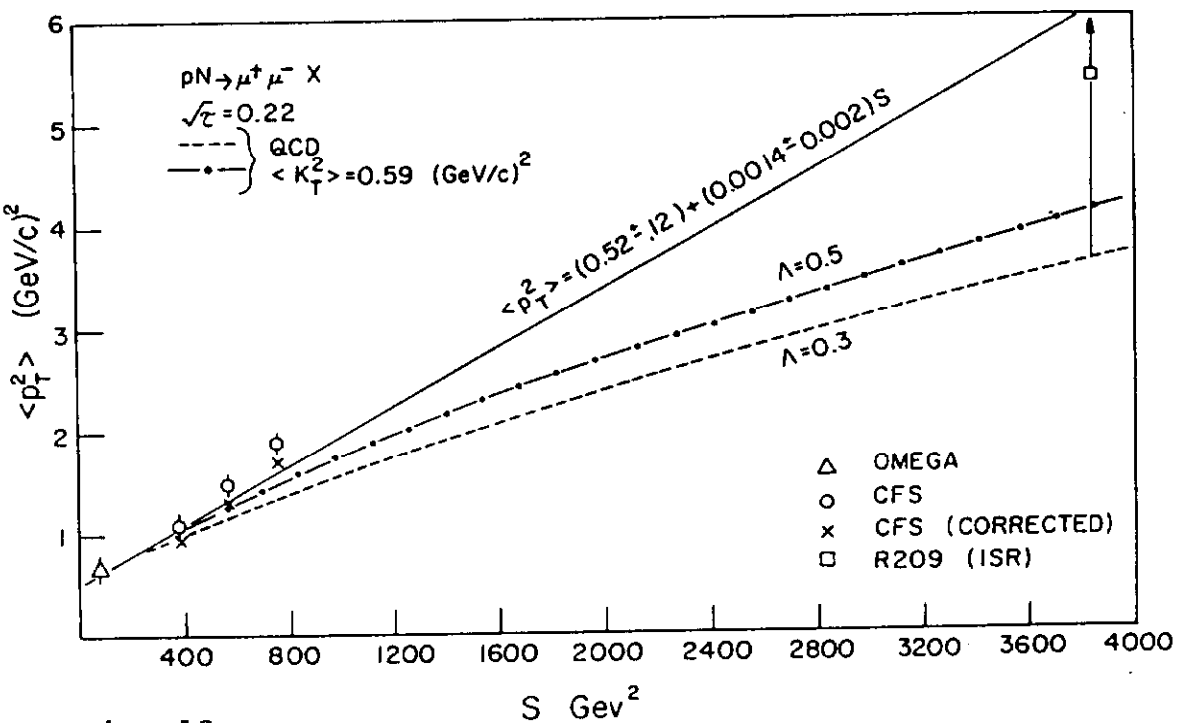
pN→μ⁺μ⁻ X
√τ=0.22
QCD
<K_T²>=0.59 (GeV/c)²
<p_T²>=(0.52±.12)+(0.0014±0.002)S
Λ=0.5
Λ=0.3
△ OMEGA
○ CFS
× CFS (CORRECTED)
□ R209 (ISR)
<p_T²> (GeV/c)²
S Gev²

Fig. 18

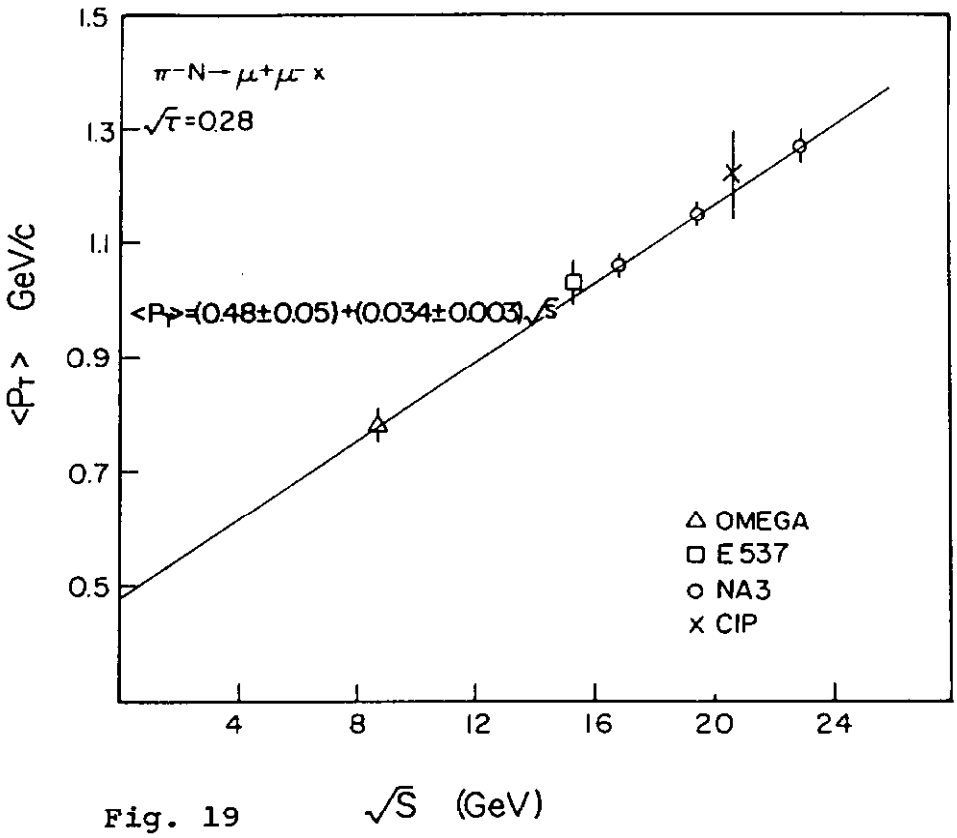
π⁻N→μ⁺μ⁻x
√τ=0.28
<P_T>=(0.48±0.05)+(0.034±0.003)√S
△ OMEGA
□ E537
○ NA3
× CIP
<P_T> GeV/c
√S (GeV)

Fig. 19

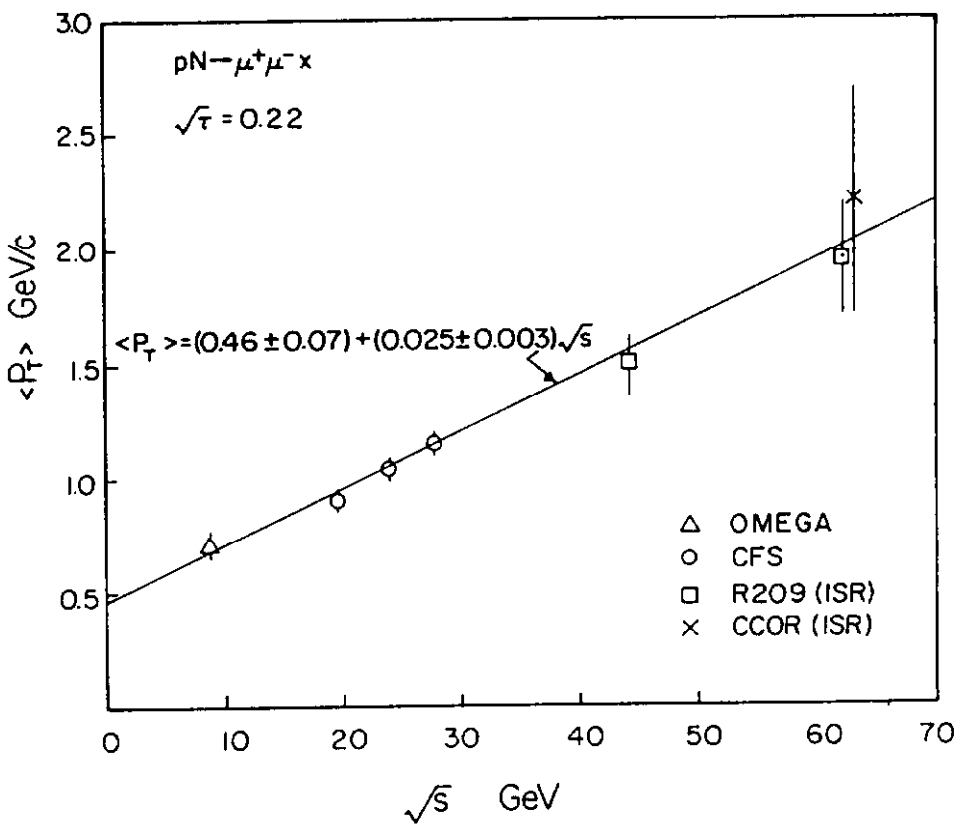
pN→μ⁺μ⁻x
√τ = 0.22
<P_T>=(0.46±0.07)+(0.025±0.003)√s
△ OMEGA
○ CFS
□ R209 (ISR)
× CCOR (ISR)
<P_T> GeV/c
√s GeV

Fig. 20